

# Fast Randomized non-Hermitian Eigensolvers Based on Rational Filtering and Matrix Partitioning

Vassilis Kalantzis, Yuanzhe Xi, and Lior Horesh

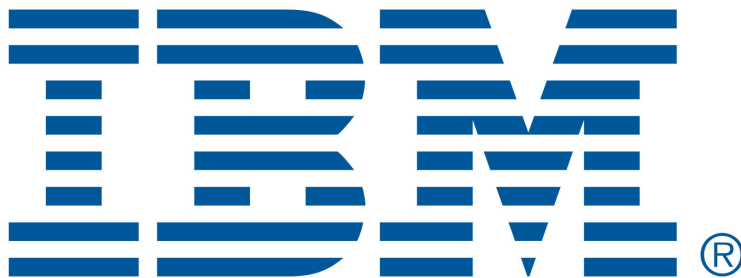
September 2021

EPrint ID: 2021.3

IBM Research  
Thomas J. Watson Research Center

Preprints available from:

<https://researcher.watson.ibm.com/researcher/view.php?person=ibm-vkal>



1 **FAST RANDOMIZED NON-HERMITIAN EIGENSOLVERS BASED**  
2 **ON RATIONAL FILTERING AND MATRIX PARTITIONING\***

3 VASSILIS KALANTZIS<sup>†</sup>, YUANZHE XI<sup>‡</sup>, AND LIOR HORESH<sup>†</sup>

4 **Abstract.** This paper describes a set of rational filtering algorithms to compute a few eigen-  
5 values (and associated eigenvectors) of non-Hermitian matrix pencils. Our interest lies in computing  
6 eigenvalues located inside a given disk, and the proposed algorithms approximate these eigenvalues  
7 and associated eigenvectors by harmonic Rayleigh-Ritz projections on subspaces built by computing  
8 range spaces of rational matrix functions through randomized range finders. These rational matrix  
9 functions are designed so that directions associated with non-sought eigenvalues are dampened to  
10 (approximately) zero. Variants based on matrix partitionings are introduced to further reduce the  
11 overall complexity of the proposed framework. Compared with existing eigenvalue solvers based on  
12 rational matrix functions, the proposed technique requires no estimation of the number of eigenvalues  
13 located inside the disk. Several theoretical and practical issues are discussed, and the competitiveness  
14 of the proposed framework is demonstrated via numerical experiments.

15 **Key words.** Rational filtering, matrix partitioning, contour integral eigensolvers, non-Hermitian  
16 eigenvalue problems, randomized algorithms

17 **AMS subject classifications.** 65F15, 15A18, 65F50

18 **1. Introduction.** This paper describes a rational filtering framework to com-  
19 pute a few eigenvalues and associated eigenvectors of non-Hermitian eigenvalue prob-  
20 lems of the form

21 (1.1) 
$$Ax = \lambda Mx,$$

22 where the matrices  $A \in \mathbb{C}^{n \times n}$  and  $M \in \mathbb{C}^{n \times n}$  are assumed large and sparse, and the  
23 pencil  $(A, M)$  is assumed regular and diagonalizable. The focus of this paper lies in  
24 computing all eigenvalues located in the interior of a disk  $\mathcal{D}$  prescribed in the complex  
25 domain. An illustrative example is shown in Figure 1.1.

26 Rational filtering eigenvalue solvers can be seen as (harmonic) Rayleigh-Ritz pro-  
27 cedures in which the projection subspace is built by exploiting a (complex) rational  
28 transformation of the matrix pencil  $(A, M)$ . These transformations are constructed  
29 so that the gap between eigenvalues located inside the disk  $\mathcal{D}$  versus those located  
30 outside the latter is as big as possible after the transformation. Applying a projec-  
31 tion scheme to the transformed pencil can then significantly enhance the convergence  
32 towards the sought invariant subspace. The most popular approaches to construct  
33 efficient rational transformations is either via shift-and-invert or via a discretization  
34 of the Cauchy integral representation of the eigenprojector along the boundary of the  
35 disk  $\mathcal{D}$  [6, 39, 44, 45, 51, 54]. Compared to shift-and-invert, contour integral eigen-  
36 solvers are generally oblivious to the location of the sought eigenvalues inside the disk  
37  $\mathcal{D}$ , and enjoy enhanced scalability when implemented in distributed memory comput-  
38 ing environments [1, 18, 21, 24, 50]. Other rational filters, though not necessarily  
39 based on contour integration, can be found in [4, 5, 15, 25, 28, 31, 41, 47, 48, 49].

40 In this paper we consider algorithms in which the projection subspace is set  
41 equal to the column space of matrices formed after applying a rational transforma-  
42 tion to the matrix pencil  $(A, M)$ . These rational transformations are constructed so

---

\*Submitted to the editors January 8, 2022.

<sup>†</sup>IBM Research, Thomas J. Watson Research Center, Yorktown Heights, NY 10598, USA  
(vkal@ibm.com, lhoresh@us.ibm.com).

<sup>‡</sup>Department of Mathematics, Emory University, Atlanta, GA 30322, USA (yxi26@emory.edu).

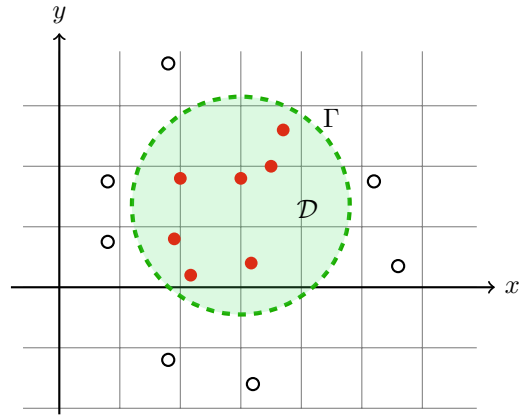


FIG. 1.1. Sought eigenvalues are denoted by red filled dots. Unwanted eigenvalues located outside the circumference  $\Gamma$  (denoted by a green dashed curve) of the disk  $\mathcal{D}$  are denoted by black solid circles.

43 that eigenvector directions associated with eigenvalues located outside the disk  $\mathcal{D}$   
 44 are approximately mapped to zero, and the corresponding column spaces are captured  
 45 through randomized range finders [33, 34]. The algorithms proposed in this paper are  
 46 also combined with matrix partitionings to reduce the computational complexity of  
 47 the construction of the projection subspace. So far matrix partitioning approaches  
 48 have been featured within the context of rational filtering only for symmetric eigen-  
 49 value problems [21, 23]. One of the main motivations of this paper is to extend this  
 50 class of techniques to non-Hermitian eigenvalue problems.

51 Overall, the proposed framework possesses the following advantages:

52 **Improved robustness.** Classical rational filtering approaches such as FEAST  
 53 [39] or the SS algorithm [44, 45] require an estimation of the number of eigenvalues  
 54 located inside the disk  $\mathcal{D}$ . However, such an estimation is not always readily available  
 55 or easy to compute for generalized eigenvalue problems. On the other hand, an  
 56 inaccurate estimation can lead to slow convergence or failure to capture all required  
 57 eigenpairs. The proposed algorithms bypass this issue by dynamically increasing the  
 58 dimension of the projection subspace.

59 **Reduced complexity.** By combining rational filtering with substructuring, the  
 60 projection subspace is formed as the direct sum of two separate subspaces approxi-  
 61 mated independently. This is done by applying a  $2 \times 2$  block partitioning to the pencil  
 62  $(A, M)$ . Two specialized algorithms are proposed to further reduce the computational  
 63 costs associated with classical rational filtering eigensolvers. The  $2 \times 2$  block parti-  
 64 tioning can be created either in an ad hoc way or by applying a graph partitioner to  
 65 the adjacency graph of the pencil  $(A, M)$ .

66 **Enhanced parallelism.** In addition to the ample opportunities for parallelism  
 67 offered by rational filtering eigensolvers, the proposed algorithms can take advantage  
 68 of an additional level of parallelism introduced by matrix substructuring.

69 The structure of this paper is organized as follows. Section 2 describes a technique  
 70 based on the combination of randomized range finders, harmonic Rayleigh-Ritz pro-  
 71 jections and rational transformations. Section 3 presents two variants based on matrix  
 72 partitioning which aim at reducing the computational cost associated with the con-  
 73 struction of an efficient projection subspace. Section 4 discusses practical details and  
 74 presents computational cost comparisons. Section 5 provides numerical experiments

75 on a few test problems. Finally, Section 6 presents our concluding remarks.

76 **1.1. Notation.** Throughout this paper we denote the spectrum of  $(A, M)$  by  
 77  $\Lambda(A, M)$ . The total number of eigenvalues located inside the disk  $\mathcal{D}$  is assumed  
 78 unknown and is denoted by  $n_{ev}$ . The eigentriplets of the matrix pencil  $(A, M)$  are  
 79 denoted by  $(\lambda_i, x^{(i)}, \hat{x}^{(i)})$ ,  $i = 1, \dots, n$ , where  $\lambda_i$  denotes the  $i$ th eigenvalue of smallest  
 80 distance from the center of the disk  $\mathcal{D}$ , and  $x^{(i)}$  and  $(\hat{x}^{(i)})^H$  denote the corresponding  
 81 right and left eigenvectors, respectively. Notice that using the above definition we  
 82 have  $\lambda_1, \dots, \lambda_{n_{ev}} \in \mathcal{D}$  and  $\lambda_{n_{ev}+1}, \dots, \lambda_n \notin \mathcal{D}$ . The superscript “ $H$ ” denotes the  
 83 conjugate transpose of the corresponding matrix. Unless mentioned otherwise, the  
 84 term “eigenvector” should be understood to refer to a right eigenvector. Throughout  
 85 the rest of this paper we use the notation  $\mathbf{rank}(X)$ ,  $\mathbf{orth}(X)$ , and  $\mathbf{range}(X)$  to denote  
 86 the rank, orthonormalization, and range (column space) of the  $m \times n$  matrix  $X$ ,  
 87 respectively. Moreover, we use the notation  $\mathbf{span}(r^{(1)}, \dots, r^{(k)})$  to denote the linear  
 88 span of vectors  $r^{(1)}, \dots, r^{(k)}$ .

89 **2. Harmonic Rayleigh-Ritz projections and randomized range finders**  
 90 **for column spaces of matrix functions.** Computing a few exterior eigenvalues  
 91 and associated eigenvectors of large and sparse matrix pencils is typically achieved  
 92 via applying a Rayleigh-Ritz procedure (RR) onto a (nearly) invariant subspace as-  
 93 sociated with the sought eigenvalues [37]. For Hermitian eigenvalue problems, the  
 94 RR procedure retains several optimality properties, e.g., see [29]. For non-Hermitian  
 95 eigenvalue problems no such optimality is guaranteed, e.g., when the sought eigenval-  
 96 ues are located in the interior of the spectrum, e.g., inside a disk  $\mathcal{D}$  surrounded by  
 97 several unwanted eigenvalues, the RR procedure might provide poor results [36].

98 An alternative for the solution of interior eigenvalue problems is the harmonic  
 99 Rayleigh-Ritz procedure (HRR) suggested in [35]. More specifically, let matrix  $Z$   
 100 represent a basis of some projection subspace  $\mathcal{Z}$ . The HRR procedure extracts ap-  
 101 proximate eigenpairs of the form  $(\theta, Zq)$  by solving the following eigenvalue problem

$$102 \quad (2.1) \quad Z^H(A - \zeta_c M)^H(A - \zeta_c M)Zq = (\theta - \zeta_c)Z^H(A - \zeta_c M)^H M Zq, \quad \zeta_c \in \mathbb{C}.$$

103 For eigenvalue problems such as the ones considered in this paper, it is reasonable to  
 104 set  $\zeta_c$  equal to the center of the disk  $\mathcal{D}$ . The approximate eigenvalue  $\theta$  and eigenvector  
 105  $Zq$  are referred to as (harmonic) Ritz value and Ritz vector, respectively. In practice, if  
 106 the subspace  $\mathcal{Z}$  includes the sought invariant subspace, then (2.1) will return accurate  
 107 approximations of the corresponding eigenpairs provided that there are no spurious  
 108 eigenvalues close to the Ritz values located inside the disk  $\mathcal{D}$  [19, 35].

109 Based on the above discussion, we seek to compute a subspace  $\mathcal{Z}$  which includes  
 110 the invariant subspace associated with  $n_{ev}$  sought eigenvalues  $\lambda_1, \dots, \lambda_{n_{ev}}$ . This sec-  
 111 tion considers ansatz subspaces of the form  $\mathcal{Z} = \mathbf{range}(\rho(M^{-1}A))$  for some scalar  
 112 function  $\rho$  such that  $\rho(M^{-1}A)$  is rank-deficient. The rest of this section considers such  
 113 a function  $\rho$  while it also discusses a randomized algorithm to compute the range of  
 114 rank-deficient matrices.

115 **2.1. Fast randomized range finder for rank-deficient matrices.** Let  $X \in$   
 116  $\mathbb{C}^{m \times n}$  be a rectangular matrix. The goal of a range finding procedure is to compute  
 117 an orthonormal matrix  $Y$  such that  $\|(I - YY^H)X\|$  is zero. In this paper we are  
 118 interested in scenarios where matrix  $X$  is rank-deficient and accessible only through  
 119 a Matrix-Vector product routine.

120 Let  $k \in \mathbb{N}$ ,  $k < \min(m, n)$ , denote the rank of matrix  $X$ . The range of matrix  
 121  $X$  is equal to the span of the left-singular vectors corresponding to the  $k$  non-zero

122 singular values. The span of these left-singular vectors can be computed in a matrix-  
 123 free fashion by Lanczos bidiagonalization (LBD) [14]. In the absence of round-off  
 124 errors, LBD requires  $k$  Matrix-Vector products with each of the matrices  $X$  and  $X^H$ ,  
 125 in addition to the cost introduced by the chosen orthogonalization strategy, e.g., see  
 126 [17]. Alternatively, we can apply  $k$  steps of the Lanczos process on  $XX^H$  [26], but  
 127 this approach still requires  $2k$  Matrix-Vector products overall.

ALGORITHM 2.1. *Randomized range finding algorithm*

0. Inputs:  $X \in \mathbb{C}^{m \times n}$ ,  $Y := 0$   
 1a. For  $i = 1, \dots, \min(m, n)$   
 2. Fill  $r \in \mathbb{C}^n$  with normally distributed random entries  
 3.  $Y = [Y, Xr]$   
 4. Set the  $i \times 1$  vector  $\sigma^{(Y)}$  equal to the (sorted) singular  
 values of matrix  $Y$   
 5. If  $\sigma_i^{(Y)} / \sigma_1^{(Y)} \leq$  machine epsilon, break;  
 1b. End  
 6. Orthonormalize and return  $Y$

129 The complexity of the range finding problem can be reduced by considering techni-  
 130 ques from randomized linear algebra [12, 30, 34]. Randomized numerical algorithms  
 131 have gained significant prominence over the last two decades due to their superior  
 132 performance in several important numerical linear algebra problems, e.g., low-rank  
 133 matrix approximations [16, 32] and principal component analysis [8, 40]. Returning  
 134 to the range finding problem, let  $R \in \mathbb{C}^{n \times k}$  be a matrix whose entries are drawn from  
 135 a Gaussian distribution. Then, with probability one, we have  $\text{rank}(XR) = k$  and  
 136  $\text{range}(XR) = \text{range}(X)$  [33]. Thus, a randomized range finder requires only half of  
 137 the Matrix-Vector products performed by LBD or Lanczos. Our interest lies in sce-  
 138 narios where the exact rank of matrix  $X$  is either unknown or expensive to estimate.  
 139 To bypass this issue, next we consider a modification of the randomized range finder  
 140 where the Matrix-Vector products with matrix  $X$  are performed in an incremental  
 141 manner and no information regarding  $k$  is needed.

142 Let  $r^{(i)} \in \mathbb{C}^n$ ,  $i = 1, 2, \dots$ , denote a sequence of vectors with normally randomly  
 143 distributed entries, and  $[Xr^{(1)}, Xr^{(2)}, \dots]$  denote the evolving matrix in which we  
 144 accumulate the products of matrix  $X$  with  $r^{(i)}$ . After  $k$  such products, the rank  
 145 (and range) of the evolving matrix is equal to that of matrix  $X$ . Since the following  
 146 Matrix-Vector products  $Xr^{(i)}$ ,  $i = k + 1, k + 2, \dots$ , already lie in  $\text{range}(X)$ , the  
 147 evolving matrix will become singular. Therefore, we can bypass the unknown rank  
 148 of matrix  $X$  by monitoring the singular values of the evolving matrix. The above  
 149 approach is listed as Algorithm 2.1. The procedure terminates when the ratio of the  
 150 smallest to the largest singular value of the matrix  $[Xr^{(1)}, Xr^{(2)}, \dots]$  becomes zero,  
 151 which in a numerical computing environment translates to smaller than or equal to  
 152 the machine epsilon.<sup>1</sup> In the absence of round-off errors, Algorithm 2.1 terminates  
 153 after  $k + 1$  iterations. The SVD of the evolving matrix in Step 3 can be updated  
 154 on-the-fly each time a new column is added [22, 55]. We note here that Algorithm 2.1  
 155 can be also seen as a variation of the adaptive range finder described in [16, Section  
 156 4] with the exception that the stopping criterion is based on the magnitude of the  
 157 condition number of the evolving matrix.

<sup>1</sup>We consider a number to be equal to zero if its numerical value is less than the machine epsilon of the IEEE 754 binary64 definition.

158 While our interest lies in computing the exact  $\mathbf{range}(X)$ , in practice we stop the  
 159 iterative procedure in Algorithm 2.1 when the ratio of the smallest to the largest  
 160 singular value becomes less than a small threshold, e.g.,  $10^{-12}$ . This helps to avoid  
 161 orthonormalizing an ill-conditioned basis at the last step of Algorithm 2.1, e.g., see  
 162 [13]. If Algorithm 2.1 terminates after  $k_0 + k_1 < k + 1$  iterations, then, with probability  
 163 at least  $1 - 6k_1^{-k_1}$ , the matrix  $Y = \mathbf{orth}(X [r^{(1)}, \dots, r^{(k_0+k_1)}])$  satisfies [16]:

$$164 \quad (2.2) \quad \|(I - YY^H)X\|_2 \leq \left(1 + 11\sqrt{k_0 + k_1}\sqrt{\min(m, n)}\right) \sigma_{k_0+1}(X),$$

165 where  $\sigma_j(X)$  denotes the  $j$ th singular value of matrix  $X$ . Therefore, when the sin-  
 166 gular values of matrix  $X$  decay fast enough, Algorithm 2.1 can still return a good  
 167 approximation of  $\mathbf{range}(X)$  in less than  $k + 1$  iterations. Note though that we can  
 168 not predict the number of iterations associated with a higher stop tolerance  
 169 in Algorithm 2.1.

170 **2.2. Column spaces of matrix functions as projection subspaces.** Let  
 171  $\rho : \mathbb{C}^* \rightarrow \mathbb{R}$ ,  $\mathbb{C}^* \subseteq \mathbb{C}$ , be a scalar function that is defined over  $\Lambda(A, M)$ . Since  $(A, M)$   
 172 is diagonalizable, applying the function  $\rho$  to matrix  $M^{-1}A$  is equivalent to

$$173 \quad (2.3) \quad \rho(M^{-1}A) = \sum_{i=1}^n \rho(\lambda_i) x^{(i)} \left(\hat{x}^{(i)}\right)^H M.$$

174 Notice now that  $\mathbf{span}(x^{(1)}, \dots, x^{(n_{ev})}) \subseteq \mathbf{range}(\rho(M^{-1}A))$  for any function  $\rho$  such  
 175 that  $\rho(\lambda_i) \neq 0$ ,  $i = 1, \dots, n_{ev}$ . Algorithm 2.2 outlines a two-step procedure to  
 176 approximate the eigenvalues located inside the disk  $\mathcal{D}$  and associated eigenvectors.  
 177 The first step is to compute an orthonormal basis matrix  $Z$  of  $\mathbf{range}(\rho(M^{-1}A))$   
 178 by calling Algorithm 2.1. The number of iterations performed by Algorithm 2.1 is  
 179 bounded by the number of eigenvalues  $\lambda$  that satisfy  $\rho(\lambda) \neq 0$ . Therefore, the scalar  
 180 function  $\rho$  should be set such that  $\rho(\lambda_i)$  is about equal to machine precision for as  
 181 many eigenvalues  $\lambda_i \notin \mathcal{D}$  as possible. The second step is to perform a HRR projection  
 182 step to approximate the eigenvalues located inside  $\mathcal{D}$  and their associated eigenvectors.  
 183 Note that no information about the value of  $n_{ev}$  is required.

ALGORITHM 2.2. *Prototype algorithm*

- 184
0. *Inputs:*  $\rho : \mathbb{C} \rightarrow \mathbb{R}$ ,  $\mathcal{D}$
  1. *Compute an orthonormal basis  $Z$  of  $\mathbf{range}(\rho(M^{-1}A))$   
by Algorithm 2.1*
  2. *Solve the eigenvalue problem in (2.1) and return all  
Ritz values  $\theta \in \mathcal{D}$  and associated Ritz vectors*

185 Motivated by the above discussion, an ideal function  $\rho$  is defined by the contour  
 186 integral

$$187 \quad (2.4) \quad \mathcal{P}(\zeta) = \frac{-1}{2\pi i} \int_{\Gamma} \frac{1}{\zeta - \nu} d\nu,$$

188 where the complex contour  $\Gamma$  denotes the circumference of the disk  $\mathcal{D}$ , and the inte-  
 189 gration is performed counter-clockwise. By Cauchy's residue theorem it follows that  
 190  $\mathcal{P}(\zeta) = 1$  for any  $\zeta \in \mathcal{D}$ , and zero otherwise. Applying (2.4) to (2.3) yields

$$191 \quad (2.5) \quad \mathcal{P}(M^{-1}A) = \frac{-1}{2\pi i} \int_{\Gamma} (M^{-1}A - \nu I)^{-1} d\nu = \sum_{i=1}^{n_{ev}} x^{(i)} \left(\hat{x}^{(i)}\right)^H M.$$

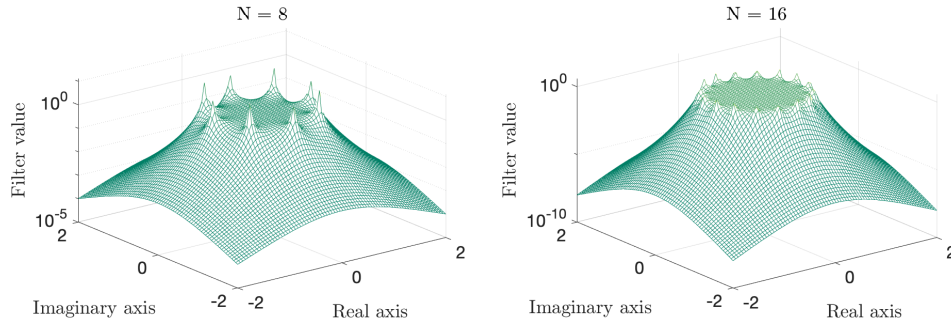


FIG. 2.1. The modulus of the rational filter  $\rho(\zeta)$  defined on the unit disk with the trapezoidal rule of order  $N = 8$  (left) and  $N = 16$  (right).

192 Algorithm 2.2 then terminates after exactly  $n_{ev}$  iterations.

193 In practice, (2.4) will be approximated by numerical quadrature which leads to a  
 194 rational “filter” function of the form

$$195 \quad (2.6) \quad \rho(\zeta) = \sum_{j=1}^N \frac{\omega_j}{\zeta - \zeta_j},$$

196 where the integer  $N$  denotes the order of the approximation, and the complex pairs  
 197  $\{\omega_j, \zeta_j\}_{j=1, \dots, N}$  denote the weights and nodes of the quadrature rule, respectively.  
 198 Rational filter functions of this form were pioneered in the context of eigenvalue  
 199 solvers first in [2, 6, 39, 44]. The application of (2.6) to the pencil  $(A, M)$  then gives

$$200 \quad (2.7) \quad \rho(M^{-1}A) = \sum_{j=1}^N \omega_j (M^{-1}A - \zeta_j I)^{-1} = \sum_{j=1}^N \omega_j (A - \zeta_j M)^{-1} M,$$

201 and computing  $\rho(M^{-1}A)r$  for a vector  $r$  at each iteration of Algorithm 2.2 involves: a)  
 202 one Matrix-Vector product with matrix  $M$ , and b) the solution of one linear system  
 203 with each matrix  $A - \zeta_j M$ ,  $j = 1, \dots, N$ . These  $N$  linear system solutions can  
 204 be obtained in parallel by replicating matrices  $A$  and  $M$  in  $N$  different groups of  
 205 processors.

206 Ideally, the function in (2.6) should decay to zero as  $\zeta$  moves away from  $\mathcal{D}$ . Figure  
 207 2.1 plots the modulus of a rational filter  $\rho(\zeta)$  defined on the unit disk ( $\mathcal{D} \equiv \{|z| : |z| \leq$   
 208  $1\}$ ) with the trapezoidal rule of order  $N = 8$  (left) and  $N = 16$  (right). Increasing  
 209 the value of  $N$  leads to a faster decay of the rational filter  $\rho(\zeta)$  outside the boundary  
 210 of  $\mathcal{D}$ . In particular, the approximation of  $\mathcal{P}(\zeta)$  by  $\rho(\zeta)$  at the center of the disk  $\mathcal{D}$   
 211 converges exponentially<sup>2</sup> with respect to  $N$  [3, 46].

212 The convergence of Algorithm 2.1 is likely to be slow for small values of  $N$  since  
 213  $\text{range}(\rho(M^{-1}A))$  could contain many eigenvector directions associated with a large  
 214 number of eigenvalues located outside  $\mathcal{D}$ . As a result, subspace iteration might be a  
 215 better alternative in this case, and this is exploited in the FEAST eigenvalue solver  
 216 library [38, 39]. The drawback of subspace iteration as a projection scheme is that  
 217 a good estimation of  $n_{ev}$  is necessary (e.g., see [10, 52, 53]), a condition which is  
 218 bypassed by Algorithm 2.2.

<sup>2</sup>Note that eigenvalues  $\lambda$  located very close to the poles  $\zeta_j$  can lead to values  $\rho(\lambda)$  which are larger than one even if  $\lambda \notin \mathcal{D}$ .

219 Throughout the rest of this paper we describe two variants which aim at reducing  
220 the computational cost of Algorithm 2.2.

221 **3. Algorithms based on matrix partitionings.** Let  $d, s \in \mathbb{N}$ , such that  
222  $n = s + d$ , and partition each eigenvector  $x^{(i)}$ ,  $i = 1, \dots, n$ , of the pencil  $(A, M)$  as

$$223 \quad (3.1) \quad x^{(i)} = \begin{pmatrix} u^{(i)} \\ y^{(i)} \end{pmatrix}, \quad u^{(i)} \in \mathbb{C}^d, \quad y^{(i)} \in \mathbb{C}^s.$$

224 In addition, let  $0_{\chi, \psi}$  denote the zero matrix of size  $\chi \times \psi$ . Then, we can write

$$225 \quad (3.2) \quad \text{span} \left( x^{(1)}, \dots, x^{(n_{ev})} \right) = \text{span} \left( \begin{bmatrix} u^{(1)}, \dots, u^{(n_{ev})} \\ 0_{s, n_{ev}} \end{bmatrix} + \begin{bmatrix} 0_{d, n_{ev}} \\ y^{(1)}, \dots, y^{(n_{ev})} \end{bmatrix} \right)$$

$$226 \quad (3.3) \quad \subseteq \text{span} \left( \begin{bmatrix} u^{(1)}, \dots, u^{(n_{ev})} \\ 0_{s, n_{ev}} \end{bmatrix} \right) \oplus \text{span} \left( \begin{bmatrix} 0_{d, n_{ev}} \\ y^{(1)}, \dots, y^{(n_{ev})} \end{bmatrix} \right).$$

228 The expression in (3.2) implies that  $\text{span} \left( x^{(1)}, \dots, x^{(n_{ev})} \right)$  is captured by the direct  
229 sum of  $\text{span} \left( u^{(1)}, \dots, u^{(n_{ev})} \right)$  and  $\text{span} \left( y^{(1)}, \dots, y^{(n_{ev})} \right)$ . The rest of this section de-  
230 scribes two variations of Algorithm 2.2, presented in Sections 3.2 and 3.3. These  
231 algorithms make use of matrix partitioning to reduce the computational costs associ-  
232 ated with the construction of a good HRR projection subspace.

233 **3.1. Two equivalent matrix resolvent representations.** Consider the fol-  
234 lowing  $2 \times 2$  block-partitioning of the non-Hermitian matrices  $A$  and  $M$ :

$$235 \quad (3.4) \quad A = \begin{pmatrix} B & F \\ E & C \end{pmatrix} \quad \text{and} \quad M = \begin{pmatrix} M_B & M_F \\ M_E & M_C \end{pmatrix},$$

236 where  $B, M_B \in \mathbb{C}^{d \times d}$ ,  $F, M_F \in \mathbb{C}^{d \times s}$ ,  $E, M_E \in \mathbb{C}^{s \times d}$ , and  $C, M_C \in \mathbb{C}^{s \times s}$ .  
237 Moreover, define the following matrix-valued functions of  $\zeta \in \mathbb{C}$ :

$$238 \quad B(\zeta) = B - \zeta M_B, \quad F(\zeta) = F - \zeta M_F, \quad E(\zeta) = E - \zeta M_E, \quad \text{and} \quad C(\zeta) = C - \zeta M_C.$$

239 For any  $\zeta \notin \Lambda(A, M)$ , the matrix  $(A - \zeta M)^{-1}$  can be written as

$$240 \quad (3.5) \quad (A - \zeta M)^{-1} = \begin{pmatrix} B(\zeta)^{-1} [I + F(\zeta)S(\zeta)^{-1}E(\zeta)B(\zeta)^{-1}] & -B(\zeta)^{-1}F(\zeta)S(\zeta)^{-1} \\ -S(\zeta)^{-1}E(\zeta)B(\zeta)^{-1} & S(\zeta)^{-1} \end{pmatrix},$$

241 where the  $s \times s$  matrix-valued function

$$242 \quad S(\zeta) = C(\zeta) - E(\zeta)B(\zeta)^{-1}F(\zeta)$$

243 is the *Schur complement* of matrix  $A - \zeta M$ . Combining (3.5) with (2.7) then gives  
(3.6)

$$244 \quad \rho(M^{-1}A) = \sum_{j=1}^N \omega_j \begin{bmatrix} B(\zeta_j)^{-1} [I + F(\zeta_j)S(\zeta_j)^{-1}E(\zeta_j)B(\zeta_j)^{-1}] & -B(\zeta_j)^{-1}F(\zeta_j)S(\zeta_j)^{-1} \\ -S(\zeta_j)^{-1}E(\zeta_j)B(\zeta_j)^{-1} & S(\zeta_j)^{-1} \end{bmatrix} M.$$

245 Similarly, the matrix  $(A - \zeta_j M)^{-1}$  can be expressed in terms of the eigenvectors  
246 of the matrix pencil  $(A, M)$  as

$$247 \quad (3.7) \quad (A - \zeta_j M)^{-1} = \sum_{i=1}^n \frac{x^{(i)} (\hat{x}^{(i)})^H}{\lambda_i - \zeta_j}.$$



248 Then, by partitioning the left eigenvectors of the pencil  $(A, M)$  as in (3.1),

$$249 \quad \left(\hat{x}^{(i)}\right)^H = \left[\left(\hat{u}^{(i)}\right)^H \quad \left(\hat{y}^{(i)}\right)^H\right], \quad \left(\hat{u}^{(i)}\right)^H \in \mathbb{C}^{1 \times d}, \quad \left(\hat{y}^{(i)}\right)^H \in \mathbb{C}^{1 \times s},$$

250 and combining (2.7) with (3.7), we obtain the following identity:

$$251 \quad (3.8) \quad \rho(M^{-1}A) = \sum_{i=1}^n \rho(\lambda_i) \begin{bmatrix} u^{(i)} \left(\hat{u}^{(i)}\right)^H & u^{(i)} \left(\hat{y}^{(i)}\right)^H \\ y^{(i)} \left(\hat{u}^{(i)}\right)^H & y^{(i)} \left(\hat{y}^{(i)}\right)^H \end{bmatrix} M.$$

252 **3.2. First algorithm.** In this section we present an algorithm which exploits the  
253 equivalent representations of  $\rho(M^{-1}A)$  shown in (3.6) and (3.8) to build a subspace  
254 which captures  $\text{span}(u^{(1)}, \dots, u^{(n_{ev})})$  and  $\text{span}(y^{(1)}, \dots, y^{(n_{ev})})$ .

255 Equating the (1,2) and (2,2) blocks on the right-hand sides of (3.6) and (3.8) gives

$$256 \quad (3.9) \quad - \sum_{j=1}^N \omega_j B(\zeta_j)^{-1} F(\zeta_j) S(\zeta_j)^{-1} = \sum_{i=1}^n \rho(\lambda_i) u^{(i)} \left(\hat{y}^{(i)}\right)^H,$$

$$\sum_{j=1}^N \omega_j S(\zeta_j)^{-1} = \sum_{i=1}^n \rho(\lambda_i) y^{(i)} \left(\hat{y}^{(i)}\right)^H.$$

257 These identities indicate that, under mild conditions, we can capture a superset of  
258  $\text{span}(u^{(1)}, \dots, u^{(n_{ev})})$  and  $\text{span}(y^{(1)}, \dots, y^{(n_{ev})})$  by capturing the range of the ma-  
259 trices on the left-hand side in (3.9).

260 **THEOREM 3.1.** Let  $[u^{(i)}]_{\rho(\lambda_i) \neq 0}$ ,  $[y^{(i)}]_{\rho(\lambda_i) \neq 0}$ , and  $[\hat{y}^{(i)}]_{\rho(\lambda_i) \neq 0}$ , denote the ma-  
261 trices whose columns are formed by those vectors  $u^{(i)}$ ,  $y^{(i)}$ , and  $\hat{y}^{(i)}$ , for which  $\rho(\lambda_i) \neq$   
262  $0$ ,  $i = 1, \dots, n$ , respectively. If the rank of matrices  $\sum_{j=1}^N \omega_j B(\zeta_j)^{-1} F(\zeta_j) S(\zeta_j)^{-1}$   
263 and  $\sum_{j=1}^N \omega_j S(\zeta_j)^{-1}$  is equal to that of matrices  $[u^{(i)}]_{\rho(\lambda_i) \neq 0}$  and  $[y^{(i)}]_{\rho(\lambda_i) \neq 0}$ , re-  
264 spectively, then:

$$265 \quad (3.10) \quad \text{range} \left( [u^{(i)}]_{\rho(\lambda_i) \neq 0} \right) = \text{range} \left( \sum_{j=1}^N \omega_j B(\zeta_j)^{-1} F(\zeta_j) S(\zeta_j)^{-1} \right),$$

266 and

$$267 \quad (3.11) \quad \text{range} \left( [y^{(i)}]_{\rho(\lambda_i) \neq 0} \right) = \text{range} \left( \sum_{j=1}^N \omega_j S(\zeta_j)^{-1} \right).$$

*Proof.* First, notice that  $\text{range} \left( [\rho(\lambda_i) u^{(i)}]_{\rho(\lambda_i) \neq 0} \right) = \text{range} \left( [u^{(i)}]_{\rho(\lambda_i) \neq 0} \right)$ , and  
 $\text{range} \left( [\rho(\lambda_i) y^{(i)}]_{\rho(\lambda_i) \neq 0} \right) = \text{range} \left( [y^{(i)}]_{\rho(\lambda_i) \neq 0} \right)$ . Second, we have

$$\sum_{j=1}^N \omega_j B(\zeta_j)^{-1} F(\zeta_j) S(\zeta_j)^{-1} = [\rho(\lambda_i) u^{(i)}]_{\rho(\lambda_i) \neq 0} [\hat{y}^{(i)}]_{\rho(\lambda_i) \neq 0}^H,$$

and

$$\sum_{j=1}^N \omega_j S(\zeta_j)^{-1} = [\rho(\lambda_i) y^{(i)}]_{\rho(\lambda_i) \neq 0} [\hat{y}^{(i)}]_{\rho(\lambda_i) \neq 0}^H.$$

268 Recall now that for two matrices  $X_1$  and  $X_2$ , if the rank of the matrix  $X_1 X_2$  is equal  
 269 to that of  $X_1$ , then the span of the columns of  $X_1$  is equal to the range of  $X_1 X_2$ . The  
 270 results in (3.10) and (3.11) follow directly by setting  $X_1 = [\rho(\lambda_i)u^{(i)}]_{\rho(\lambda_i) \neq 0}$  in (3.10)  
 271 and  $X_1 = [\rho(\lambda_i)y^{(i)}]_{\rho(\lambda_i) \neq 0}$  in (3.11), respectively, while  $X_2 = [\hat{y}^{(i)}]_{\rho(\lambda_i) \neq 0}^H$ .  $\square$

272 Theorem 3.1 implies that a necessary condition for (3.10) and (3.11) to hold is

$$273 \quad (3.12) \quad \max \left( \text{rank} \left( \begin{bmatrix} u^{(i)} \\ \rho(\lambda_i) \neq 0 \end{bmatrix} \right), \text{rank} \left( \begin{bmatrix} y^{(i)} \\ \rho(\lambda_i) \neq 0 \end{bmatrix} \right) \right) \leq \text{rank} \left( \begin{bmatrix} \hat{y}^{(i)} \\ \rho(\lambda_i) \neq 0 \end{bmatrix} \right).$$

274 For symmetric eigenvalue problems we have  $y^{(i)} = \hat{y}^{(i)}$  and (3.12) is trivially satisfied  
 275 [20]. In practice, the violation of (3.12) for non-Hermitian eigenvalue problems is  
 276 quite rare in a finite-precision arithmetic environment.

277 Algorithm 3.1 outlines a matrix partitioning procedure to build the HRR projec-  
 278 tion subspace in (2.1) by setting the latter subspace equal to the direct sum of sub-  
 279 spaces  $\text{range} \left( \sum_{j=1}^N \omega_j B(\zeta_j)^{-1} F(\zeta_j) S(\zeta_j)^{-1} \right)$  and  $\text{range} \left( \sum_{j=1}^N \omega_j S(\zeta_j)^{-1} \right)$ . Each  
 280 instance of Algorithm 2.1 called in Algorithm 3.1 performs a number of iterations  
 281 which is at most equal to the number of eigenvalues  $\lambda$  for which  $\rho(\lambda) \neq 0$ . Moreover,  
 282 the two instances of Algorithm 2.1 shown in Steps 1 and 2 are performed in parallel  
 283 and thus the linear system solutions computed in Step 2 are exploited at Step 1 as  
 284 well. Moreover, similarly to Algorithm 2.2, Algorithm 3.1 requires no estimation of  
 285 the value of  $n_{ev}$ .

ALGORITHM 3.1.

0a. *Inputs:*  $N$ ,  $\mathcal{D}$

0b. *Compute the complex pairs*  $\{\omega_j, \zeta_j\}_{j=1,2,\dots,N}$ , *set*  $G := W := 0$

0c. *(Optionally) Reorder*  $(A, M)$  *as in Section 4.2*

- 286 1. *Compute an orthonormal basis*  $G$  *of*  $\text{range} \left( \sum_{j=1}^N \omega_j S(\zeta_j)^{-1} \right)$   
*by Algorithm 2.1*
2. *Compute an orthonormal basis*  $W$  *of*  $\text{range} \left( \sum_{j=1}^N \omega_j B(\zeta_j)^{-1} F(\zeta_j) S(\zeta_j)^{-1} \right)$   
*by Algorithm 2.1*
3. *Set*  $Z = \begin{bmatrix} W \\ G \end{bmatrix}$ , *solve the eigenvalue problem in (2.1) and return*  
*all Ritz values*  $\theta \in \mathcal{D}$  *and associated Ritz vectors*

287 Unless mentioned otherwise, the default value of the number of poles in the rati-  
 288 onal filter  $\rho$  will be equal to  $N = 16$ .

289 **3.3. Second algorithm.** This section describes an alternative technique to con-  
 290 struct the matrix  $W$  in Algorithm 3.1 under the assumption that the pencil  $(B, M_B)$   
 291 is diagonalizable. Throughout the rest of this section we will denote the eigentriplets  
 292 of the pencil  $(B, M_B)$  by  $(\delta_i, v^{(i)}, \hat{v}^{(i)})$ ,  $i = 1, 2, \dots, d$ , where  $\delta_i$  denotes the eigenvalue  
 293 of  $(B, M_B)$  with the  $i$ th shortest distance from the center of the disk  $\mathcal{D}$ , and  $v^{(i)}$  and  
 294  $(\hat{v}^{(i)})^H$  denote the corresponding right and left eigenvectors, respectively.

295 By combining (3.2) and (3.4), we can write the top  $d \times 1$  part of the eigenvector  
 296  $x^{(i)} = \begin{pmatrix} u^{(i)} \\ y^{(i)} \end{pmatrix}$  associated with the eigenvalue  $\lambda_i$  as

$$297 \quad (3.13) \quad u^{(i)} = -B(\lambda_i)^{-1} F(\lambda_i) y^{(i)}.$$

298 While expression (3.13) is not practical, it serves as a starting point for the construc-  
 299 tion of a subspace which (approximately) captures  $\text{span} (u^{(i)})$  without depending on  
 300 the (unknown) quantities  $\lambda_i$  and  $y^{(i)}$ .

Let  $G$  be a matrix such that  $y^{(i)} \in \mathbf{range}(G)$ , e.g., the matrix  $G$  constructed in Algorithm 3.1. In addition, define the matrices

$$V_\phi = \left[ v^{(1)}, v^{(2)}, \dots, v^{(\phi)} \right] \quad \text{and} \quad \hat{V}_\phi = \left[ \hat{v}^{(1)}, \hat{v}^{(2)}, \dots, \hat{v}^{(\phi)} \right],$$

301 where  $\phi \in \mathcal{Z}^*$  is larger than or equal to the number of eigenvalues of  $(B, M_B)$  located  
 302 inside the disk  $\mathcal{D}$ . Taking advantage of the identity  $I = V_\phi \hat{V}_\phi^H M_B + (I - V_\phi \hat{V}_\phi^H M_B)$ ,  
 303 and noticing that  $\mathbf{span} \left( V_\phi \hat{V}_\phi^H M_B B(\lambda_i)^{-1} F(\lambda_i) y^{(i)} \right) \subseteq \mathbf{span} \left( v^{(1)}, v^{(2)}, \dots, v^{(\phi)} \right)$ , we  
 304 can write

(3.14)

$$\begin{aligned} \mathbf{span} \left( u^{(i)} \right) &= \mathbf{span} \left( B(\lambda_i)^{-1} F(\lambda_i) y^{(i)} \right) \\ &= \mathbf{span} \left( V_\phi \hat{V}_\phi^H M_B B(\lambda_i)^{-1} F(\lambda_i) y^{(i)} + (I - V_\phi \hat{V}_\phi^H M_B) B(\lambda_i)^{-1} F(\lambda_i) y^{(i)} \right) \\ 305 &\subseteq \mathbf{span} \left( v^{(1)}, v^{(2)}, \dots, v^{(\phi)} \right) + \mathbf{span} \left( (I - V_\phi \hat{V}_\phi^H M_B) B(\lambda_i)^{-1} F(\zeta) G \right) + \\ &\quad \mathbf{span} \left( (I - V_\phi \hat{V}_\phi^H M_B) B(\lambda_i)^{-1} M_F G \right), \end{aligned}$$

where  $\zeta \in \mathcal{D}$ , and we replaced  $F(\lambda_i)$  by its equivalent form

$$F(\lambda_i) = F(\zeta) - (\lambda_i - \zeta) M_F.$$

306 The expression in (3.14) still depends on  $\lambda_i$  through the term  $B(\lambda_i)^{-1}$ . Next, we  
 307 show an equivalent expression of the matrix  $(I - V_\phi \hat{V}_\phi^H M_B) B(\lambda_i)^{-1}$ .

308 **THEOREM 3.2.** *Let  $\zeta_c \in \mathbb{C}$  be the center of disk  $\mathcal{D}$  and  $\phi \in \mathbb{N}$  larger than or equal  
 309 to the number of eigenvalues of  $(B, M_B)$  located inside  $\mathcal{D}$ . If we define the matrix*

$$310 \quad \tilde{B}(\zeta) := \left( I - V_\phi \hat{V}_\phi^H M_B \right) B(\zeta)^{-1},$$

311 then

$$312 \quad (3.15) \quad \left( I - V_\phi \hat{V}_\phi^H M_B \right) B(\lambda_i)^{-1} = \tilde{B}(\zeta_c) \sum_{k=0}^{\infty} \left[ (\lambda_i - \zeta_c) M_B \tilde{B}(\zeta_c) \right]^k,$$

313 for any  $\lambda_i \in \mathcal{D}$ .

*Proof.* Define the matrices

$$V = \left[ V_\phi, v^{(\phi+1)}, \dots, v^{(d)} \right] \quad \text{and} \quad \hat{V} = \left[ \hat{V}_\phi, \hat{v}^{(\phi+1)}, \dots, \hat{v}^{(d)} \right].$$

314 Recall that  $\hat{V}^H M_B V = I$ , and thus  $M_B = \hat{V}^{-H} V^{-1}$  and  $B = \hat{V}^{-H} \begin{pmatrix} \delta_1 & & \\ & \ddots & \\ & & \delta_d \end{pmatrix} V^{-1}$ .

315 Using the above identities we can write

$$\begin{aligned} \tilde{B}(\zeta) &= \left( I - V_\phi \hat{V}_\phi^H M_B \right) V \begin{pmatrix} \delta_1 - \zeta & & \\ & \ddots & \\ & & \delta_d - \zeta \end{pmatrix}^{-1} \hat{V}^H \\ 316 &= V \begin{pmatrix} \mathbf{0}_{\phi, \phi} & & & \\ & \frac{1}{\delta_{\phi+1} - \zeta} & & \\ & & \ddots & \\ & & & \frac{1}{\delta_d - \zeta} \end{pmatrix} \hat{V}^H. \end{aligned}$$

317 Let us now define the scalar  $\gamma_j = \frac{\lambda_i - \zeta_c}{\delta_j - \zeta_c}$ . We can write

$$318 \quad \tilde{B}(\zeta_c) \left[ (\lambda_i - \zeta_c) M_B \tilde{B}(\zeta_c) \right]^k = V \begin{pmatrix} \mathbf{0}_{\phi, \phi} & & & \\ & \frac{\gamma_{\phi+1}^k}{\delta_{\phi+1} - \zeta_c} & & \\ & & \ddots & \\ & & & \frac{\gamma_d^k}{\delta_d - \zeta_c} \end{pmatrix} \hat{V}^H.$$

319 Accounting for all powers  $k = 0, 1, 2, \dots$ , gives

$$320 \quad \tilde{B}(\zeta_c) \sum_{k=0}^{\infty} \left[ (\lambda_i - \zeta_c) M_B \tilde{B}(\zeta_c) \right]^k = V \begin{pmatrix} \mathbf{0}_{\phi, \phi} & & & \\ & \frac{\sum_{k=0}^{\infty} \gamma_{\phi+1}^k}{\delta_{\phi+1} - \zeta_c} & & \\ & & \ddots & \\ & & & \frac{\sum_{k=0}^{\infty} \gamma_d^k}{\delta_d - \zeta_c} \end{pmatrix} \hat{V}^H.$$

321 Since  $\zeta_c$  is the center of  $\mathcal{D}$ , it follows that  $|\gamma_j| < 1$  for any  $\delta_j \notin \mathcal{D}$ . Therefore,  
322 the geometric series converges and  $\sum_{k=0}^{\infty} \gamma_j^k = \frac{1}{1 - \gamma_j} = \frac{\delta_j - \zeta_c}{\delta_j - \lambda_i}$ . It follows that

$$323 \quad \frac{1}{\delta_j - \zeta_c} \sum_{k=0}^{\infty} \gamma_j^k = \frac{1}{\delta_j - \lambda_i}.$$

324 We finally have

$$325 \quad \begin{aligned} \tilde{B}(\zeta_c) \sum_{k=0}^{\infty} \left[ (\lambda_i - \zeta_c) M_B \tilde{B}(\zeta_c) \right]^k &= V \begin{pmatrix} \mathbf{0}_{\phi, \phi} & & & \\ & \frac{1}{\delta_{\phi+1} - \lambda_i} & & \\ & & \ddots & \\ & & & \frac{1}{\delta_d - \lambda_i} \end{pmatrix} \hat{V}^H \\ &= \left( I - V_{\phi} \hat{V}_{\phi}^H M_B \right) B(\lambda_i)^{-1}. \end{aligned}$$

326 This concludes the proof.  $\square$

327 Theorem 3.2 implies that we can approximate  $\left( I - V_{\phi} \hat{V}_{\phi}^H M_B \right) B(\lambda_i)^{-1}$  through  
328 a finite truncation of the right-hand side in (3.15). The approximation error of this  
329 truncation is considered in the following proposition.

330 PROPOSITION 3.3. *Let  $\psi$  be a positive integer and define the error matrix*

$$331 \quad R_{\psi}(\lambda_i) = \left( I - V_{\phi} \hat{V}_{\phi}^H M_B \right) B(\lambda_i)^{-1} - \tilde{B}(\zeta_c) \sum_{k=0}^{\psi} \left[ (\lambda_i - \zeta_c) M_B \tilde{B}(\zeta_c) \right]^k.$$

332 Then

$$333 \quad (3.16) \quad R_{\psi}(\lambda_i) = \sum_{k=\psi+1}^{\infty} \sum_{j=\phi+1}^d \left[ \frac{(\lambda_i - \zeta_c)^k}{(\delta_j - \zeta_c)^{k+1}} \right] v^{(j)} \left( \hat{v}^{(j)} \right)^H M_B.$$

334 *Proof.* Recall the scalar  $\gamma_j = \frac{\lambda_i - \zeta_c}{\delta_j - \zeta_c}$ . The matrix  $R_\psi(\lambda_i)$  is then equal to

$$335 \quad R_\psi(\lambda_i) = V \begin{pmatrix} \mathbf{0}_{\phi, \phi} & & & \\ & \frac{\sum_{k=\psi+1}^{\infty} \gamma_{\phi+1}^k}{\delta_{\phi+1} - \zeta_c} & & \\ & & \ddots & \\ & & & \frac{\sum_{k=\psi+1}^{\infty} \gamma_d^k}{\delta_d - \zeta_c} \end{pmatrix} \hat{V}^H.$$

336 The proof concludes by replacing  $\gamma_j$  with its ratio.  $\square$

337 Proposition 3.3 indicates that when  $\zeta_c$  is close to the sought eigenvalues  $\lambda_1, \dots, \lambda_{nev}$   
 338 and the eigenvalues  $\delta_{\phi+1}, \dots, \delta_d$  are located far away from the disk  $\mathcal{D}$ , then the matrix  
 339  $\tilde{B}(\zeta_c) \sum_{k=0}^{\psi} [(\lambda_i - \zeta_c) M_B \tilde{B}(\zeta_c)]^k$  can be used as an accurate approximation of the  
 340 matrix  $(I - V_\phi \hat{V}_\phi^H M_B) B(\lambda_i)^{-1}$  even for small values of  $\psi$ .

341 Based on the above discussion, we expect to find a reasonable approximation of  
 342 the subspace  $\text{span}(u^{(1)}, \dots, u^{(nev)})$  in the range of the matrix

$$343 \quad (3.17) \quad W_{\phi, \psi} = \left[ V_\phi, \underbrace{(I - V_\phi \hat{V}_\phi^H M_B) \hat{B}_\psi(\zeta_c) \hat{G}_F}_{\text{only if } M_F \neq 0}, \underbrace{(I - V_\phi \hat{V}_\phi^H M_B) \hat{B}_\psi(\zeta_c) \hat{G}_{M_F}}_{\text{only if } M_F \neq 0} \right],$$

344 where

$$345 \quad \hat{B}_\psi(\zeta_c) = \left[ \tilde{B}(\zeta_c), \tilde{B}(\zeta_c) [M_B \tilde{B}(\zeta_c)], \dots, \tilde{B}(\zeta_c) [M_B \tilde{B}(\zeta_c)]^\psi \right],$$

346 and we set

$$347 \quad \hat{G}_F = \begin{bmatrix} F(\zeta_c)G & & & \\ & F(\zeta_c)G & & \\ & & \ddots & \\ & & & F(\zeta_c)G \end{bmatrix}, \quad \hat{G}_{M_F} = \begin{bmatrix} M_F G & & & \\ & M_F G & & \\ & & \ddots & \\ & & & M_F G \end{bmatrix}.$$

**ALGORITHM 3.2.**

- 0a. *Inputs:*  $N$ ,  $\mathcal{D}$ ,  $\psi$  (optionally),  $\phi$  (optionally)  
 0b. *Compute the complex pairs*  $\{\omega_j, \zeta_j\}_{j=1,2,\dots,N}$ , *set*  $G := 0$   
 0c. (Optionally) *Reorder*  $(A, M)$  *as in Section 4.2*  
 1. *Compute an orthonormal basis*  $G$  *of*  $\text{range} \left( \sum_{j=1}^N \omega_j S(\zeta_j)^{-1} \right)$   
 348 *by Algorithm 2.1*  
 2. *Compute the eigenpairs associated with the*  $\phi$  *eigenvalues of smallest*  
*modulus of the pencil*  $(B(\zeta), M_B)$  *and form the matrix*  $V_\phi$   
 3. *Set the matrix*  $W_{\phi, \psi}$  *as in (3.17)*  
 4. *Set*  $Z = \begin{bmatrix} W_{\phi, \psi} \\ G \end{bmatrix}$ , *solve the eigenvalue problem in (2.1) and return*  
*all Ritz values*  $\theta \in \mathcal{D}$  *and associated Ritz vectors*

349 The complete algorithmic procedure is summarized in Algorithm 3.2. The ac-  
 350 curacy in the approximation of the eigenpairs  $(\lambda_i, x^{(i)})$ ,  $i = 1, \dots, nev$ , depends on

TABLE 4.1

Total number of linear system solutions of the form  $B(\zeta)x_d = b_d$  and  $S(\zeta)x_s = b_s$  computed by Algorithm 2.2, Algorithm 3.1, Algorithm 3.2, and the algorithm used in the FEAST software package. The variables  $\eta_1 \in \mathbb{N}$ ,  $\eta_2 \in \mathbb{N}$ ,  $\eta_3 \in \mathbb{N}$ , denote the number of iterations performed by Algorithm 2.1 when called from Algorithm 2.2, Algorithm 3.1, and Algorithm 3.2, respectively. The variable  $\tau_\phi$  denotes the number of linear systems of the form  $B(\zeta_c)x_d = b_d$  required to compute the  $\phi$  sought eigenvectors of the pencil  $(B - \zeta_c M_B, M_B)$  by Implicitly Restarted Arnoldi (IRA) combined with shift-and-invert [27]. The variable  $\eta_4 \in \mathbb{N}$  denotes the number of iterations performed by subspace iteration.

	Alg. 2.2	Alg. 3.1	Alg. 3.2		Sub. It.
			$M_F = 0$	$M_F \neq 0$	
$B(\zeta)x_d = b_d$	$2N\eta_1$	$N\eta_2$	$\eta_3(\psi + 1) + \tau_\phi$	$2\eta_3(\psi + 1) + \tau_\phi$	$2mN\eta_4$
$S(\zeta)x_s = b_s$	$N\eta_1$	$N\eta_2$	$N\eta_3$	$N\eta_3$	$mN\eta_4$

351 the distance of the eigenvalues  $\lambda_i \in \mathcal{D}$  from both the center of the disk  $\mathcal{D}$  and the  
 352 (non-deflated) eigenvalues of the matrix pencil  $(B, M_B)$ . In contrast, the accuracy  
 353 provided by Algorithm 3.1 is irrespective to the location of the eigenvalues  $\lambda_i \in \mathcal{D}$ .  
 354 Thus, the latter should be the algorithm of choice when one seeks higher accuracy in  
 355 the approximation of the  $n_{ev}$  sought eigenpairs of the pencil  $(A, M)$ . On the other  
 356 hand, Algorithm 3.2 should be preferred when a few digits of accuracy are deemed  
 357 enough, and lower wall-clock execution time is critical.

358 Compared to Algorithm 3.1, Algorithm 3.2 introduces two new parameters,  $\psi \in \mathbb{N}$   
 359 and  $\phi \in \mathbb{N}$ . Larger values of these two integers lead to higher accuracy but increase the  
 360 associated computational cost. Increasing the value of  $\psi$  aims at reducing the error  
 361 along all eigenvector directions of  $(B, M_B)$ , while increasing the value of  $\phi$  aims at  
 362 eliminating the approximation error associated with eigenvectors corresponding closer  
 363 to the center of the disk  $\mathcal{D}$ . Generally speaking, the main improvements in accuracy  
 364 come from increasing the value of  $\psi$ . Our default choice is to set  $\psi = 1$ , and  $\phi$  equal to  
 365 the number of eigenvalues of the pencil  $(B, M_B)$  located inside the disk  $\mathcal{D}$ . If additional  
 366 accuracy is needed, one can augment  $W_{\phi, \psi}$  with either additional eigenvectors of the  
 367 pencil  $(B, M_B)$  (i.e., increase  $\phi$ ), or additional resolvent approximation matrix terms  
 368 (i.e., increase  $\psi$ ) and only repeat the Rayleigh-Ritz projection step. This approach  
 369 can be repeated more than once, i.e., until the residual norms of all  $n_{ev}$  approximate  
 370 eigenpairs are less a chosen threshold.

## 371 4. Practical details.

372 **4.1. Computational cost comparison.** The main computational bottleneck  
 373 of the rational filtering algorithms discussed in this paper is the solution of complex-  
 374 shifted sparse linear systems of the form  $B(\zeta)x_d = b_d$  and  $S(\zeta)x_s = b_s$ . Therefore, an  
 375 algorithm that requires fewer such linear system solutions will typically be faster as  
 376 well.

377 Table 4.1 summarizes the computational costs of Algorithm 2.2, Algorithm 3.1,  
 378 and Algorithm 3.2, where we assume that all linear systems are solved by a direct  
 379 solver and their complexity is oblivious to the actual value of  $\zeta \notin \Lambda(B, M_B)$ . The  
 380 variables  $\eta_1 \in \mathbb{N}$ ,  $\eta_2 \in \mathbb{N}$ ,  $\eta_3 \in \mathbb{N}$ , denote the number of iterations performed by  
 381 Algorithm 2.1 when called from Algorithm 2.2, Algorithm 3.1, and Algorithm 3.2,  
 382 respectively. It is straightforward to observe that when  $\eta_1 \approx \eta_2 \approx \eta_3$ , Algorithm 3.1  
 383 requires about half linear system solutions of the form  $B(\zeta)x_d = b_d$  than what Algo-  
 384 rithm 2.2 does. Moreover, Algorithm 3.2 requires a number of linear system solutions

385 which is independent of the number of poles  $N$ . Thus, larger values of  $N$  should  
 386 increase the computational complexity gap in favor of Algorithm 3.2. For comparison  
 387 purposes we also list the computational complexity of subspace iteration applied to  
 388 matrix  $\rho(M^{-1}A)$  with an initial subspace of dimension  $m \geq n_{ev}$ . In contrast to the  
 389 algorithms proposed in this paper, the convergence of subspace iteration depends on  
 390 the dimension  $m$  of its initial subspace.

391 **4.2. Matrix partitionings.** The matrix partitioning algorithms discussed in  
 392 this paper can take advantage of a reordering of the pencil  $(A, M)$  so that the pencil  
 393  $(B, M_B)$  is block-diagonal. For Algorithm 3.2 this implies that the computation of the  
 394 matrix  $V_\phi$  then decouples into  $p$  independent generalized non-Hermitian eigenvalue  
 395 problems. The eigenvalues of each one of these  $p$  matrix pencils can be then computed  
 396 in parallel.

397 To obtain the above reordering we partition the adjacency graph of the matrix  
 398  $|A| + |A^T| + |M| + |M^T|$  into  $p \geq 2$  non-overlapping partitions [42]. We then reorder  
 399 the equations/unknowns so that the interior variables across all partitions are ordered  
 400 before the interface ones. The latter procedure is equivalent to transforming the  
 401 original pencil  $(A, M)$  into the form  $(PAP^T, PMP^T)$ , where the  $n \times n$  matrix  $P$   
 402 holds the row permutation of  $(A, M)$ . The eigenpairs of  $(A, M)$  are connected with  
 403 those of the matrix pencil  $(PAP^T, PMP^T)$  through the formula

$$404 \quad PAP^T \left( Px^{(i)} \right) = \lambda_i PMP^T \left( Px^{(i)} \right).$$

405 The matrices  $PAP^T$  and  $PMP^T$  can be written as

$$406 \quad PAP^T = \begin{pmatrix} B_1 & & & F_1 \\ & B_2 & & F_2 \\ & & \ddots & \vdots \\ & & & B_p & F_p \\ E_1 & E_2 & \dots & E_p & C \end{pmatrix}, \quad PMP^T = \begin{pmatrix} M_B^{(1)} & & & M_F^{(1)} \\ & M_B^{(2)} & & M_F^{(2)} \\ & & \ddots & \vdots \\ & & & M_B^{(p)} & M_F^{(p)} \\ M_E^{(1)} & M_E^{(2)} & \dots & M_E^{(p)} & M_C \end{pmatrix}$$

407 where matrices  $B_i$  and  $M_B^{(i)}$  are square matrices of size  $d_i \times d_i$ , matrices  $F_i$  ( $E_i$ ) and  
 408  $M_F^{(i)}$  ( $M_E^{(i)}$ ) are of size  $d_i \times s_i$  ( $s_i \times d_i$ ), and the integers  $d_i$  and  $s_i$  denote the number  
 409 of interior and interface nodes located in the  $i$ th subdomain of the adjacency graph  
 410 of  $|A| + |A^T| + |M| + |M^T|$ , respectively. On the other hand, matrices  $C$  and  $M_C$  are  
 411 of size  $s \times s$  where  $s = \sum_{i=1}^p s_i$ .

412 **5. Experiments.** The numerical experiments presented in this section were per-  
 413 formed in a Matlab environment (version R2018b), using 64-bit arithmetic, on a single  
 414 core of a MacBook Pro equipped with a quad-core 2.5 GHz Intel Core i7 processor  
 415 and 16 GB 1600 MHz DDR3 of system memory. The matrices used throughout our  
 416 experiments are listed in Table 5.1 and can be retrieved from SuiteSparse Matrix  
 417 Collection [9] and Matrix Market repository [7].

418 Throughout the rest of this section we consider the application of three different  
 419 algorithms: a) Algorithm 3.1, b) Algorithm 3.2, and finally c) subspace iteration with  
 420 the matrix  $\rho(M^{-1}A)$ , where the initial subspace is of dimension  $m \geq n_{ev}$ . We will  
 421 refer to this approach as RSI. As a separate note, a high-performance implementation  
 422 of subspace iteration with rational filtering can be found in the FEAST software  
 423 package.

TABLE 5.1  
*n*: size of matrices *A* and *M*, *nnz*(.): number of nonzero entries.

#	Matrix pencil	<i>n</i>	<i>nnz</i> ( <i>A</i> )/ <i>n</i>	<i>nnz</i> ( <i>M</i> )/ <i>n</i>	Application
1.	<b>bfw782</b>	782	9.6	7.6	Engineering
2.	<b>utm1700b</b>	1,700	12.7	1.0	Electromagnetics
3.	<b>wang1</b>	2,903	6.6	1.0	Semiconductors
4.	<b>rdb32001</b>	3,200	5.9	1.0	CFD
5.	<b>thermal</b>	3,456	19.2	1.0	Thermal
6.	<b>dw4096</b>	8,192	5.1	1.0	Engineering
7.	<b>big</b>	13,209	6.9	1.0	Directed weighted graph

424 The radius of the disk  $\mathcal{D}$  is set equal to 1.001 times the radius of the minimal  
425 enclosing circle of eigenvalues  $\lambda_1, \dots, \lambda_{n_{ev}}$ . The rational filter function in (2.6) is  
426 constructed through discretizing (2.4) by the trapezoidal rule of order  $N$ . Throughout  
427 the rest of this section we assume that the iterative loop in Algorithm 2.1 terminates  
428 when the ratio of the smallest to the largest singular value is less than or equal to  
429  $1.0 \times 10^{-12}$ , and we set a maximum number of four hundred iterations. All matrix  
430 pencils were reordered as discussed in Section 4.2 using  $p = 8$ . The residual norm  
431 of each approximate eigenpair  $(\hat{\lambda}, \hat{x})$  is computed as  $\hat{\rho} = \frac{\|A\hat{x} - \hat{\lambda}M\hat{x}\|_2}{\|A\hat{x}\|_2 + |\hat{\lambda}|\|M\hat{x}\|_2}$ . All  
432 algorithms discussed in this section return only those approximate eigenpairs  $(\hat{\lambda}, \hat{x})$   
433 for which  $\hat{\lambda} \in \mathcal{D}$ . When more than  $n_{ev}$  approximate eigenvalues are located in  $\mathcal{D}$  we  
434 purge the spurious ones by keeping only those for which the associated residual norm  
435 is smaller than the threshold tolerance  $1.0 \times 10^{-3}$ . This approach was successful in  
436 all experiments we performed.

437 **5.1. A detailed example.** We consider the computation of the  $n_{ev} = 20$  eigen-  
438 values of smallest modulus (and their associated eigenvectors) of the matrices **wang1**  
439 and **thermal**. The size of the Schur complement matrices after the application of the  
440 graph partitioner is equal to  $s = 576$ , and  $s = 668$ , respectively. The application of  
441 Algorithm 3.1 is visualized in Figure 5.1. The first row of plots shows the  $n_{ev}$  sought  
442 and  $n_{ev}$  immediate unwanted eigenvalues of smallest modulus, while the second row  
443 of shows the ratio of the smallest to the largest singular value as determined at each  
444 iteration of Algorithm 2.1 during its application to matrix  $\sum_{j=1}^N \omega_j S(\zeta_j)^{-1}$ .<sup>3</sup> Notice  
445 that this ratio approximates zero and decreases faster for larger values of  $N$  as a  
446 consequence of the fact that the rank of the matrix  $\sum_{j=1}^N \omega_j S(\zeta_j)^{-1}$  approaches that  
447 of the matrix  $\sum_{i=1}^{n_{ev}} y^{(i)} (\hat{y}^{(i)})^H$ , which is bounded from above by  $n_{ev}$ . Increasing the  
448 value of  $N$  does not always lead to a proportional gain in terms of convergence rate.  
449 For example, increasing  $N = 8$  to  $N = 16$  reduces the number of iterations by a factor  
450 of at least four for the first two matrices considered. On the other hand, increasing  
451  $N = 16$  to  $N = 32$  reduces the number of iterations by a factor which is smaller than  
452 two. Moreover, small values of  $N$ , e.g.,  $N = 4$ , might lead to very slow convergence.  
453 The third and fourth rows of plots show the associated eigenvalue errors (left col-  
454 umn) and residual norms (right column) returned by Algorithm 3.1. For the choice  
455  $N = 4$ , the range of matrices  $\sum_{j=1}^N \omega_j B(\zeta_j)^{-1} F(\zeta_j) S(\zeta_j)^{-1}$  and  $\sum_{j=1}^N \omega_j S(\zeta_j)^{-1}$  was  
456 not captured to high precision and this is reflected in the approximation of the sought  
457 eigenpairs. For the choices  $N = 8$ , 16 and  $N = 32$ , the range of both matrices was

<sup>3</sup>Results for matrix  $\sum_{j=1}^N \omega_j B(\zeta_j)^{-1} F(\zeta_j) S(\zeta_j)^{-1}$  were essentially identical and thus not reported.



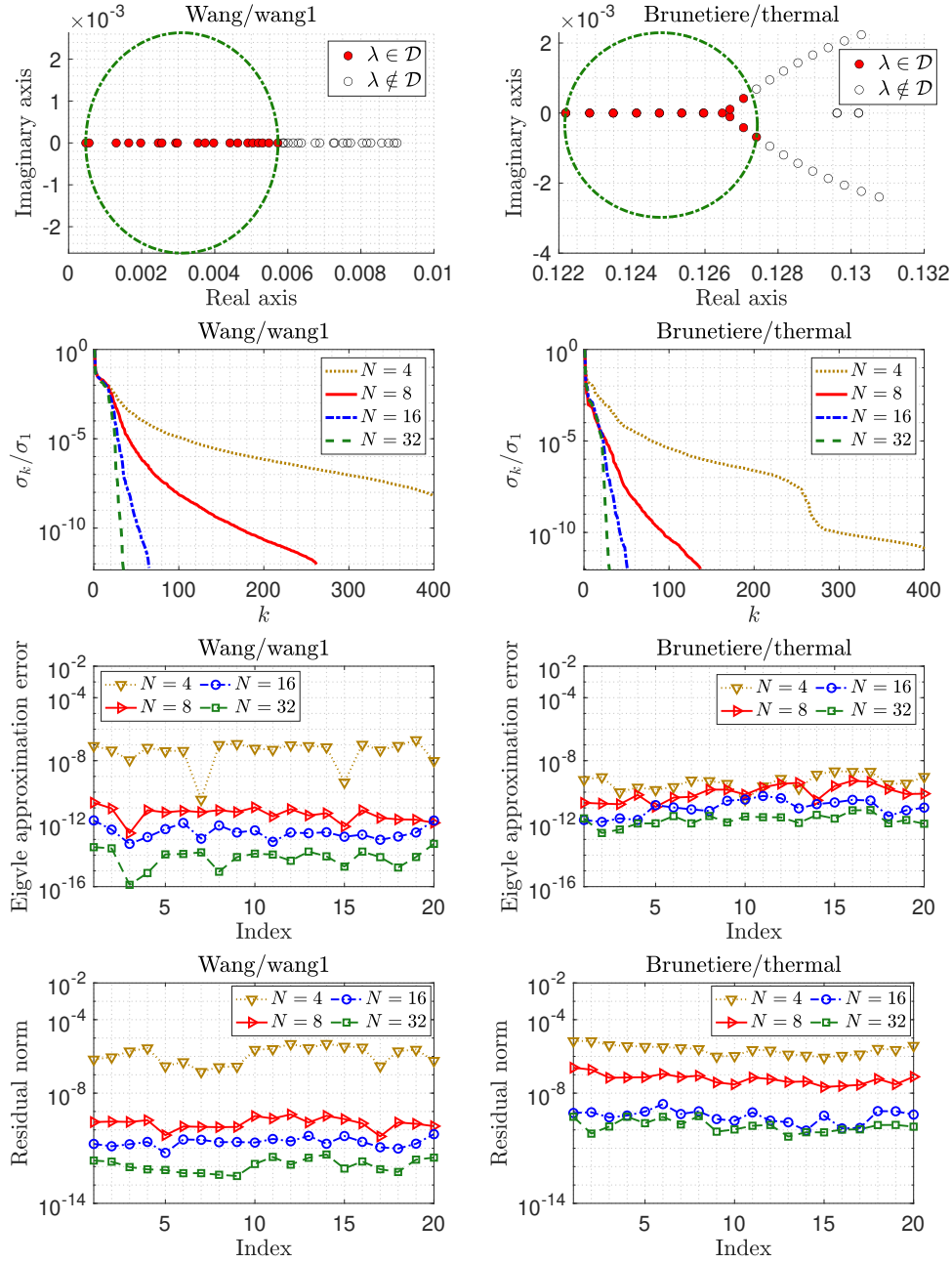


FIG. 5.1. Application of Algorithm 3.1 to matrices *wang1* (left column) and *thermal* (right column). First row: the  $n_{ev}$  sought eigenvalues of  $(A, M)$  and  $n_{ev}$  immediate unwanted eigenvalues of smallest modulus. Second row: the ratio of smallest to largest singular value of matrix  $G$  as determined at each iteration of Algorithm 2.1 during its application to matrix  $\sum_{j=1}^N \omega_j S(\zeta_j)^{-1}$ . Third row: absolute eigenvalue error. Fourth row: residual norm. The indices of the  $x$ -axis are organized such that index ‘ $i$ ’ corresponds to the sought eigenvalue with the  $i$ th smallest real part.

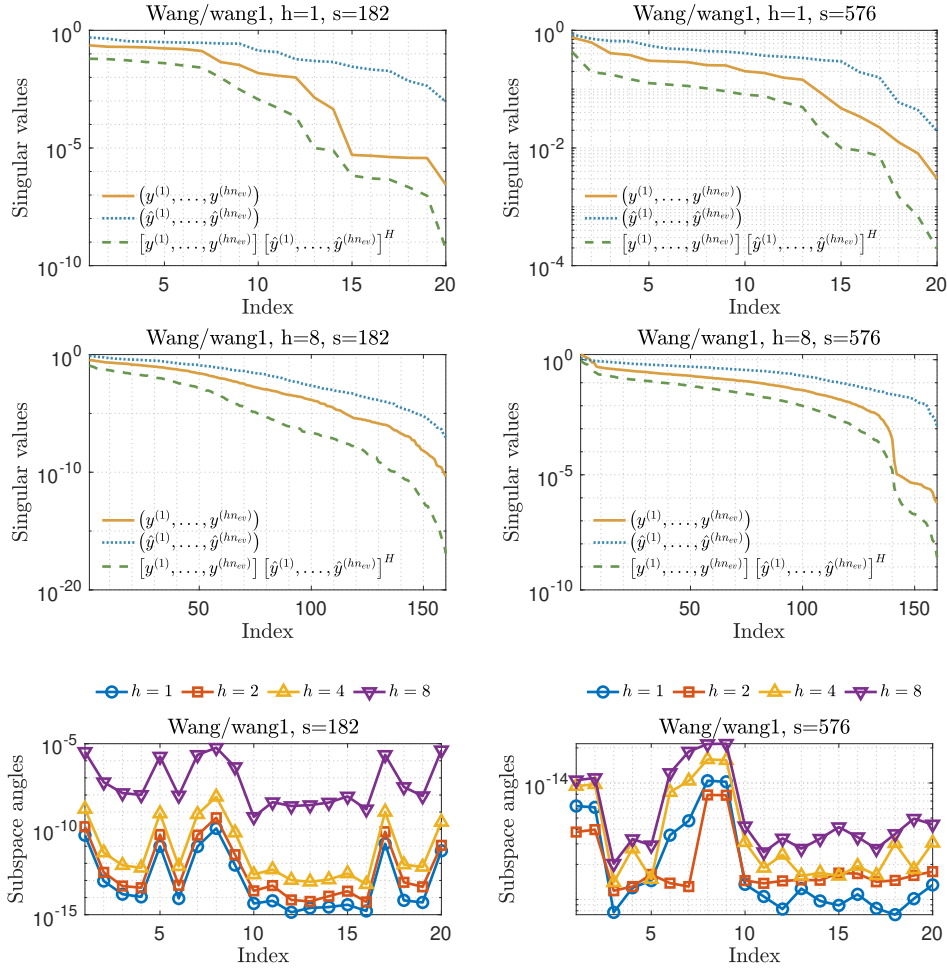


FIG. 5.2. Singular values of matrices  $[y^{(1)}, \dots, y^{(hn_{ev})}]$ ,  $[\hat{y}^{(1)}, \dots, \hat{y}^{(hn_{ev})}]$ , and their product  $[y^{(1)}, \dots, y^{(hn_{ev})}] [\hat{y}^{(1)}, \dots, \hat{y}^{(hn_{ev})}]^H$ , for different values of  $h \in \mathbb{N}$  and size  $s$  of the matrix  $\sum_{j=1}^N \omega_j S(\zeta_j)^{-1}$ . In all figures we set  $n_{ev} = 20$ . First row:  $h = 1$  and matrix  $A$  was partitioned so that the size of each Schur complement matrix in  $\sum_{j=1}^N \omega_j S(\zeta_j)^{-1}$  is equal to  $s = 182$  (left) and  $s = 576$  (right). Second row: same as before but now we set  $h = 8$ . Third row: angles between  $\text{range}([y^{(1)}, \dots, y^{(hn_{ev})}] [\hat{y}^{(1)}, \dots, \hat{y}^{(hn_{ev})}]^H)$  and vectors  $y^{(1)}, \dots, y^{(n_{ev})}$ .

458 captured up to the required tolerance and the sought eigenpairs were captured to  
 459 higher accuracy.

460 The results in Figure 5.1 suggest that larger values of  $N$  can lead to higher accu-  
 461 racy in Algorithm 3.1 even though the range of matrices  $\sum_{j=1}^N \omega_j B(\zeta_j)^{-1} F(\zeta_j) S(\zeta_j)^{-1}$   
 462 and  $\sum_{j=1}^N \omega_j S(\zeta_j)^{-1}$  is captured highly accurately for all  $N = 8$ ,  $N = 16$ , and  $N = 32$ .  
 463 Consider for example the matrix  $\sum_{j=1}^N \omega_j S(\zeta_j)^{-1} = [\rho(\lambda_i) y^{(i)}]_{\rho(\lambda_i) \neq 0} [\hat{y}^{(i)}]^H$ . In  
 464 practice, even though the condition in Proposition 3.1 holds, some of the trailing non-  
 465 zero singular values of the matrix  $\sum_{j=1}^N \omega_j S(\zeta_j)^{-1}$  might be (much) smaller than those  
 466 of  $[\rho(\lambda_i) y^{(i)}]_{\rho(\lambda_i) \neq 0}$ , thus “suppressing” some directions of  $\text{span}([\rho(\lambda_i) y^{(i)}]_{\rho(\lambda_i) \neq 0})$

467 in the range of the matrix  $\sum_{j=1}^N \omega_j S(\zeta_j)^{-1}$ . Since these directions generally have a  
 468 nonzero projection to the subspace  $\text{span}(y^{(1)}, \dots, y^{(n_{ev})})$ , we expect that the accuracy  
 469 to which we can capture the latter subspace might also be reduced. The same holds  
 470 for  $\text{span}(u^{(1)}, \dots, u^{(n_{ev})})$  and the range of matrix  $\sum_{j=1}^N \omega_j B(\zeta_j)^{-1} F(\zeta_j) S(\zeta_j)^{-1}$  as  
 471 well.

472 Figure 5.2 visualizes the above discussion for matrix `wang1`. In particular, we  
 473 plot the singular values of the matrices  $[y^{(1)}, \dots, y^{(n_{ev})}]$ ,  $[\hat{y}^{(1)}, \dots, \hat{y}^{(n_{ev})}]$ , as well  
 474 as those of their matrix product, for  $h = 1$  and  $h = 8$ , and  $n_{ev} = 20$ . Smaller  
 475 values of  $h$  simulate larger values of  $N$ . The size of the Schur complement ma-  
 476 trices was varied as  $s = 182$  and  $s = 576$ . Observe that the singular values of  
 477 the matrix  $[y^{(1)}, \dots, y^{(n_{ev})}] [\hat{y}^{(1)}, \dots, \hat{y}^{(n_{ev})}]^H$  trail those of  $[y^{(1)}, \dots, y^{(n_{ev})}]$ . As  
 478 a result, some directions of  $\text{span}(y^{(1)}, \dots, y^{(n_{ev})})$  are captured less accurately in  
 479  $\text{range}([y^{(1)}, \dots, y^{(n_{ev})}] [\hat{y}^{(1)}, \dots, \hat{y}^{(n_{ev})}]^H)$ . The latter effect is sketched in the  
 480 bottom row of plots where we plot the angle between the vectors  $y^{(1)}, \dots, y^{(n_{ev})}$  and  
 481  $\text{range}([y^{(1)}, \dots, y^{(n_{ev})}] [\hat{y}^{(1)}, \dots, \hat{y}^{(n_{ev})}]^H)$ . Ideally, all angles should be equal to  
 482 zero. However, we observe larger angles when  $h$  is larger (i.e.,  $N$  gets smaller) and  
 483 the vectors  $y^{(i)}$  and  $\hat{y}^{(i)}$  lie in a lower-dimensional subspace (i.e.,  $s$  gets smaller).

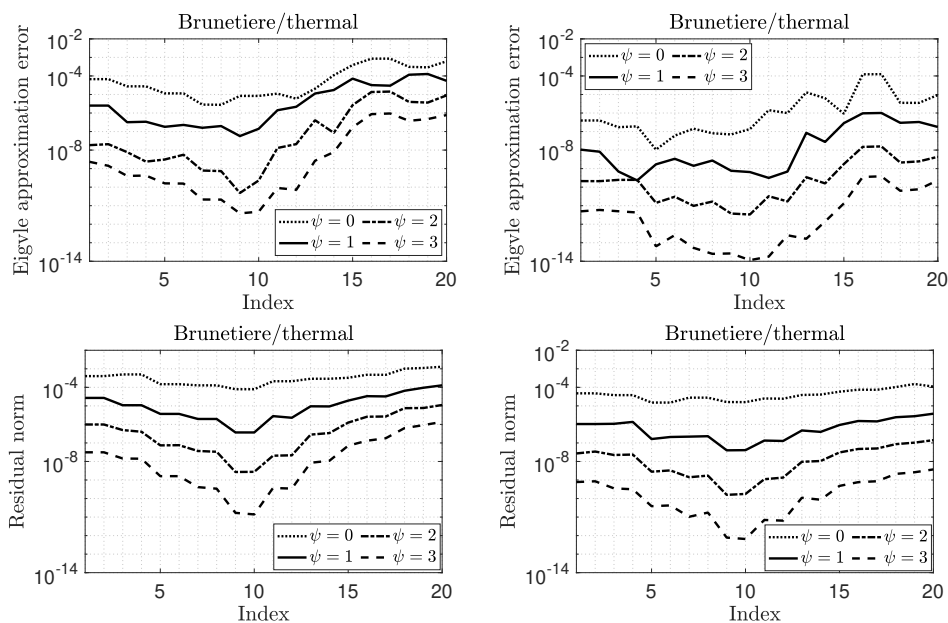


FIG. 5.3. Application of Algorithm 3.2 to the *thermal* matrix. Top row: absolute eigenvalue errors for different values of  $\psi$  and  $\phi = 14$  (left) and  $\phi = 160$  (right). Bottom row: residual norms for the same values. The indices of the x-axis are organized such that index ‘ $i$ ’ corresponds to the sought eigenvalue with the  $i$ th smallest real part.

484 Figure 5.3 plots the eigenvalue approximation errors and corresponding residual  
 485 norms in the approximation of the  $n_{ev}$  smallest modulus eigenvalues and associated  
 486 eigenvectors of the `thermal` matrix by Algorithm 3.2. The number of computed  
 487 matrix resolvent terms was set to  $\psi = 0, 1, 2$ , and  $\psi = 3$ , while the number of  
 488 computed (deflated) eigenvectors was varied to  $\phi = 14$  and  $\phi = 160$ . The choice  
 489  $\phi = 14$  coincides with computing only those eigenvalues of the pencil  $(B, M_B)$  located

490 inside the disk  $\mathcal{D}$ . The number of poles was set equal to  $N = 16$ .<sup>4</sup> As expected, the  
 491 accuracy in the approximation of the sought eigenpairs improves with larger values of  
 492  $\psi$  since the action of the matrix  $(I - V_\phi \hat{V}_\phi^H M_B) B(\lambda_i)^{-1}$  is now approximated more  
 493 accurately. Similarly, increasing  $\phi = 14$  to  $\phi = 160$  leads to enhanced accuracy. Note  
 494 that the major improvements in accuracy come from increasing the value of  $\psi$ . This  
 495 was a general trend observed for the rest of our test matrices as well. Moreover, as  
 496 was also discussed in Section 3.3, the accuracy obtained by Algorithm 3.2 depends on  
 497 the location of each eigenvalue  $\lambda_i \in \mathcal{D}$  since the action of  $(I - V_\phi \hat{V}_\phi^H M_B) B(\lambda_i)^{-1}$   
 498 is better approximated for those  $\lambda_i \in \mathcal{D}$  located closer to the center of the disk  $\mathcal{D}$ .  
 499 This is in contrast to Algorithm 3.1 which provides an almost uniform accuracy for  
 500 all eigenpairs  $(\lambda_i, x^{(i)})$  for which  $\lambda_i \in \mathcal{D}$ .

501 **5.2. Comparisons against subspace iteration with rational filtering.** We  
 502 now consider the computation of the  $n_{ev} = 40$  eigenvalues of smallest modulus (and  
 503 their associated eigenvectors) of the matrix pencil `bfw782`, and the matrices `utm1700b`,  
 504 `rdb32001`, `dw4096`, and `big`. Figure 5.4 plots the  $2n_{ev}$  eigenvalues of smallest modulus  
 of the last four matrices. Table 5.2 lists the maximum and minimum absolute

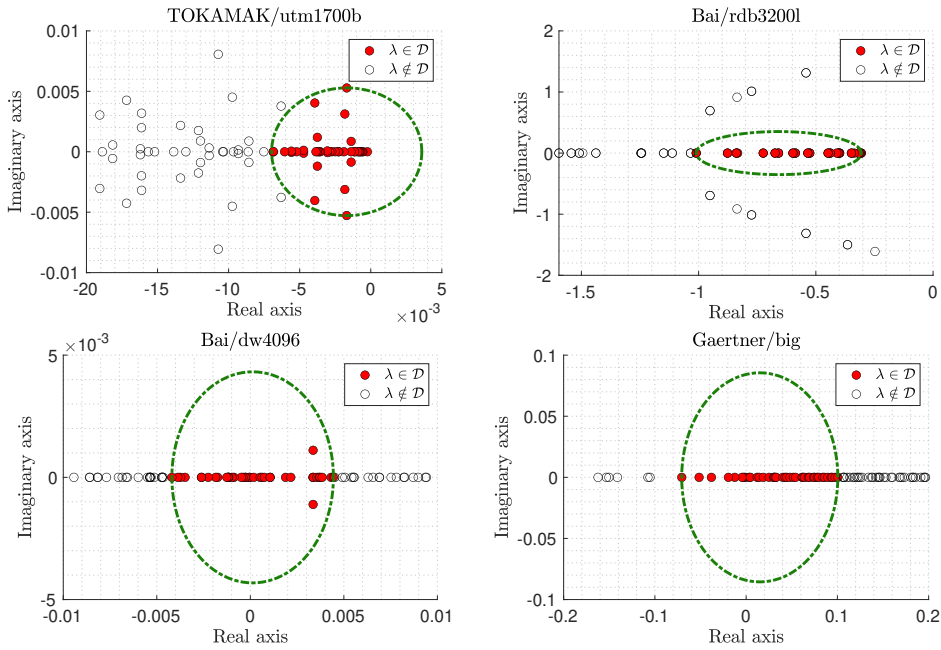


FIG. 5.4. Plot of the  $2n_{ev}$  eigenvalues of smallest modulus of some of the matrices listed in Table 5.1.

505

506 eigenvalue errors and associated residual norms returned by Algorithm 3.1 as  $N$  varies.  
 507 The number of iterations performed by Algorithm 3.1 is also listed. As expected,  
 508 larger values of  $N$  lead to fewer iterations since the rational filter  $\rho(\zeta)$  decays faster  
 509 outside  $\mathcal{D}$ . In agreement with the results discussed in Figure 5.2, larger values of  $N$   
 510 also lead to higher accuracy. Additionally, Table 5.3 lists the maximum eigenvalue

<sup>4</sup>The results obtained for the choices  $N = 8$  and  $N = 32$  were essentially identical to those for the case  $N = 16$ , and thus are not reported.

TABLE 5.2

Minimum and maximum eigenvalue errors and residual norms returned by Algorithm 3.1 for the test matrices listed in Table 5.1. The total number of iterations performed by Algorithm 3.1 is also reported. A value ‘F’ indicates that the loop in Algorithm 3.1 did not terminate within four hundred iterations.

		Algorithm 3.1					
		$\min  \lambda - \hat{\lambda} $	$\max  \lambda - \hat{\lambda} $	$\min \hat{\rho}$	$\max \hat{\rho}$	It	
bfw782	$N = 4$	$4.3 \times 10^{-1}$	$2.1 \times 10^{-0}$	$3.2 \times 10^{-2}$	$2.4 \times 10^{-1}$	87	
	$N = 8$	$1.5 \times 10^{-2}$	$3.2 \times 10^{-1}$	$2.9 \times 10^{-4}$	$2.0 \times 10^{-2}$	87	
	$N = 16$	$1.3 \times 10^{-7}$	$4.5 \times 10^{-4}$	$5.9 \times 10^{-8}$	$1.0 \times 10^{-6}$	76	
	$N = 32$	$1.1 \times 10^{-9}$	$7.4 \times 10^{-6}$	$6.6 \times 10^{-10}$	$2.8 \times 10^{-8}$	55	
utm1700b	$N = 4$	$1.4 \times 10^{-8}$	$1.3 \times 10^{-4}$	$2.0 \times 10^{-7}$	$3.9 \times 10^{-6}$	235	
	$N = 8$	$1.2 \times 10^{-9}$	$3.2 \times 10^{-6}$	$6.9 \times 10^{-9}$	$2.5 \times 10^{-7}$	134	
	$N = 16$	$8.0 \times 10^{-12}$	$7.0 \times 10^{-8}$	$5.9 \times 10^{-10}$	$4.0 \times 10^{-8}$	72	
	$N = 32$	$1.6 \times 10^{-11}$	$3.1 \times 10^{-8}$	$6.6 \times 10^{-10}$	$6.0 \times 10^{-8}$	53	
rdb32001	$N = 4$	$2.0 \times 10^{-5}$	$1.7 \times 10^{-3}$	$9.1 \times 10^{-4}$	$1.5 \times 10^{-2}$	296	
	$N = 8$	$7.2 \times 10^{-9}$	$5.7 \times 10^{-4}$	$2.3 \times 10^{-7}$	$3.5 \times 10^{-6}$	161	
	$N = 16$	$1.6 \times 10^{-12}$	$3.9 \times 10^{-9}$	$7.5 \times 10^{-10}$	$4.5 \times 10^{-8}$	77	
	$N = 32$	$1.3 \times 10^{-15}$	$2.3 \times 10^{-13}$	$2.1 \times 10^{-11}$	$5.6 \times 10^{-10}$	52	
dw4096	$N = 4$	$2.4 \times 10^{-8}$	$4.0 \times 10^{-5}$	$2.9 \times 10^{-5}$	$1.4 \times 10^{-2}$	F	
	$N = 8$	$7.2 \times 10^{-12}$	$6.1 \times 10^{-9}$	$1.9 \times 10^{-8}$	$3.1 \times 10^{-5}$	329	
	$N = 16$	$2.6 \times 10^{-15}$	$1.8 \times 10^{-10}$	$2.7 \times 10^{-10}$	$5.5 \times 10^{-6}$	147	
	$N = 32$	$9.8 \times 10^{-15}$	$3.4 \times 10^{-13}$	$2.6 \times 10^{-12}$	$1.5 \times 10^{-11}$	75	
big	$N = 4$	$4.8 \times 10^{-6}$	$3.0 \times 10^{-2}$	$3.8 \times 10^{-4}$	$1.1 \times 10^{-2}$	377	
	$N = 8$	$1.5 \times 10^{-11}$	$3.6 \times 10^{-6}$	$2.1 \times 10^{-6}$	$1.2 \times 10^{-4}$	226	
	$N = 16$	$6.2 \times 10^{-13}$	$1.7 \times 10^{-9}$	$1.0 \times 10^{-8}$	$2.8 \times 10^{-6}$	108	
	$N = 32$	$1.3 \times 10^{-14}$	$6.3 \times 10^{-11}$	$1.8 \times 10^{-9}$	$1.3 \times 10^{-6}$	68	

TABLE 5.3

Maximum eigenvalue error and residual norm returned by Algorithm 3.2 for some of the test matrices listed in Table 5.1. These results were obtained by setting  $N = 16$  and varying the value of computed resolvent terms  $\psi$ .

	bfw782	utm1700b	rdb32001	wd4096	big	
$ \lambda - \hat{\lambda} $	$\psi = 0$	$9.0 \times 10^{-2}$	$5.1 \times 10^{-3}$	$1.5 \times 10^{-1}$	$2.8 \times 10^{-1}$	$7.2 \times 10^{-2}$
	$\psi = 1$	$5.9 \times 10^{-3}$	$1.0 \times 10^{-5}$	$9.1 \times 10^{-3}$	$1.2 \times 10^{-1}$	$2.0 \times 10^{-3}$
	$\psi = 2$	$1.5 \times 10^{-4}$	$2.8 \times 10^{-7}$	$2.4 \times 10^{-4}$	$2.9 \times 10^{-3}$	$1.4 \times 10^{-5}$
	$\psi = 3$	$8.4 \times 10^{-6}$	$9.0 \times 10^{-8}$	$7.5 \times 10^{-6}$	$9.7 \times 10^{-5}$	$8.9 \times 10^{-7}$
$\hat{\rho}$	$\psi = 0$	$4.3 \times 10^{-2}$	$1.2 \times 10^{-3}$	$1.0 \times 10^{-0}$	$4.6 \times 10^{-1}$	$2.6 \times 10^{-1}$
	$\psi = 1$	$4.1 \times 10^{-3}$	$4.7 \times 10^{-4}$	$6.0 \times 10^{-2}$	$4.3 \times 10^{-1}$	$1.1 \times 10^{-1}$
	$\psi = 2$	$2.4 \times 10^{-3}$	$2.8 \times 10^{-6}$	$1.6 \times 10^{-3}$	$3.0 \times 10^{-2}$	$4.0 \times 10^{-3}$
	$\psi = 3$	$3.8 \times 10^{-5}$	$6.6 \times 10^{-7}$	$7.3 \times 10^{-5}$	$1.2 \times 10^{-4}$	$6.2 \times 10^{-5}$

error and residual norm returned by Algorithm 3.2 when the value of  $\phi$  is set equal to the number of eigenvalues located inside the disk  $\mathcal{D}$  and  $\psi$  varies.

Table 5.4 lists the average number (with respect to  $N$ ) of linear systems of the form  $B(\zeta)x_d = b_d$  and  $S(\zeta)x_s = b_s$  solved by Algorithm 3.1, Algorithm 3.2, and RSI.<sup>5</sup> The loop in RSI terminates when the maximum residual in the approximation of the  $n_{ev}$  sought eigenpairs becomes smaller than or equal to the maximum residual norm achieved by Algorithm 3.1. These residual norms listed in Table 5.2. Notice that the number of linear systems  $B(\zeta)x_d = b_d$  solved by Algorithm 3.2 is independent of  $N$ , and thus the average value becomes smaller as  $N$  increases. On the other hand, the

<sup>5</sup>These numbers do not include the cost to compute a good approximation of  $n_{ev}$  in RSI.

TABLE 5.4

Average number of linear systems of the form  $B(\zeta_j)x_d = b_d$  and  $S(\zeta_j)x_s = b_s$  solved per pole  $\zeta_j$ ,  $j = 1, \dots, N$ . For Algorithm 3.2 we consider only the case  $\psi = 3$ . For RSI we set  $m := m_1 = 1.1n_{ev}$ ,  $m := m_2 = 1.5n_{ev}$ , and  $m := m_3 = 2n_{ev}$ .

		bfw782		utm1700b		rdb32001		dw4096		big	
		$B(\zeta_j)$	$S(\zeta_j)$	$B(\zeta_j)$	$S(\zeta_j)$	$B(\zeta_j)$	$S(\zeta_j)$	$B(\zeta_j)$	$S(\zeta_j)$	$B(\zeta_j)$	$S(\zeta_j)$
$N = 8$	Alg. 3.1	87	87	134	134	161	161	329	329	226	226
	Alg. 3.2	112	87	76	134	71	161	176	329	127	226
	RSI( $m_1$ )	264	132	616	308	616	308	616	308	704	352
	RSI( $m_2$ )	120	60	240	120	240	120	480	240	480	240
	RSI( $m_3$ )	160	80	320	160	320	160	320	160	320	160
$N = 16$	Alg. 3.1	76	76	72	72	77	77	147	147	108	108
	Alg. 3.2	50	76	23	72	26	77	42	147	33	108
	RSI( $m_1$ )	440	220	352	176	352	176	616	308	352	176
	RSI( $m_2$ )	360	180	120	60	240	120	240	120	240	120
	RSI( $m_3$ )	320	160	160	80	160	80	160	80	160	80
$N = 32$	Alg. 3.1	55	55	53	53	52	52	75	75	68	68
	Alg. 3.2	20	55	9	53	10	52	12	75	12	68
	RSI( $m_1$ )	264	132	176	88	264	132	616	308	352	176
	RSI( $m_2$ )	240	120	120	60	120	60	240	120	240	120
	RSI( $m_3$ )	160	80	160	80	160	80	160	80	160	80

520 accuracy achieved by Algorithm 3.2 is also lower. For RSI we consider three different  
521 dimensions of the starting subspace, set as  $m = 1.1n_{ev}$ ,  $m = 1.5n_{ev}$ , and  $m = 2n_{ev}$ .  
522 The rate of convergence of RSI is dictated by the ratio  $\rho(\lambda_m)/\rho(\lambda_{n_{ev}})$ , and thus the  
523 convergence rate improves as  $m$  increases. We observe two main trends. First, for  
524 small values of  $m$ , e.g.,  $m = 1.1n_{ev}$ , RSI is considerably more expensive than both  
525 Algorithm 3.1 and Algorithm 3.2. This is because for small values of  $m$  the ratio  
526  $\rho(\lambda_m)/\rho(\lambda_{n_{ev}})$  might not be close to zero, thus leading to slower convergence in RSI.  
527 Second, as  $m$  increases, the average number of linear systems solved by RSI generally  
528 decreases, however the large value of  $m$  might lead to a few unnecessary solves, i.e., for  
529  $N = 32$  choosing  $m = 2n_{ev}$  sometimes provides the same accuracy with  $m = 1.5n_{ev}$ .

530 In the previous experiment we assumed that the tolerance threshold in RSI was  
531 dictated by the maximum residual norm achieved by Algorithm 3.1. Since Algorithm  
532 3.1 is a one-shot method, its maximum attainable accuracy is lower than that of RSI  
533 since the latter is an iterative approach. Nonetheless, the accuracy of the approxi-  
534 mate eigenpairs returned by Algorithm 3.1 can improve by using the corresponding  
535 eigenvectors as an initial subspace in a separate run of RSI. While this enhancement  
536 comes at an increased computational cost, it is generally still cheaper than applying  
537 subspace iteration with a random starting subspace since it avoids the overhead asso-  
538 ciated with the computation of a good approximation of  $n_{ev}$  through the techniques  
539 described in [43] and [10]. Figure 5.5 plots the maximum residual norm achieved at  
540 the end of each iteration when RSI is applied to matrices utm1700b and dw4096 with  
541  $m = 1.5n_{ev}$  and  $n_{ev} = 40$ . The initial subspace in RSI was set using “a)”  $m$  random  
542 vectors as in the results reported above (dashed lines), and “b)” the  $n_{ev}$  approximate  
543 eigenvectors returned by Algorithm 3.1 augmented by  $m - n_{ev}$  random vectors (solid  
544 lines). In the latter case, the value at the origin denotes the accuracy achieved by  
545 Algorithm 3.1 before post-processing by RSI. The combination of RSI with Algorithm  
546 3.1 leads to faster convergence, since the initial subspace is of much higher quality.  
547 What approach will be faster overall depends on the particular problem. For example,  
548 choosing  $N = 8$  and a random initial subspace leads to very slow convergence in the  
549 case of matrix dw4096.

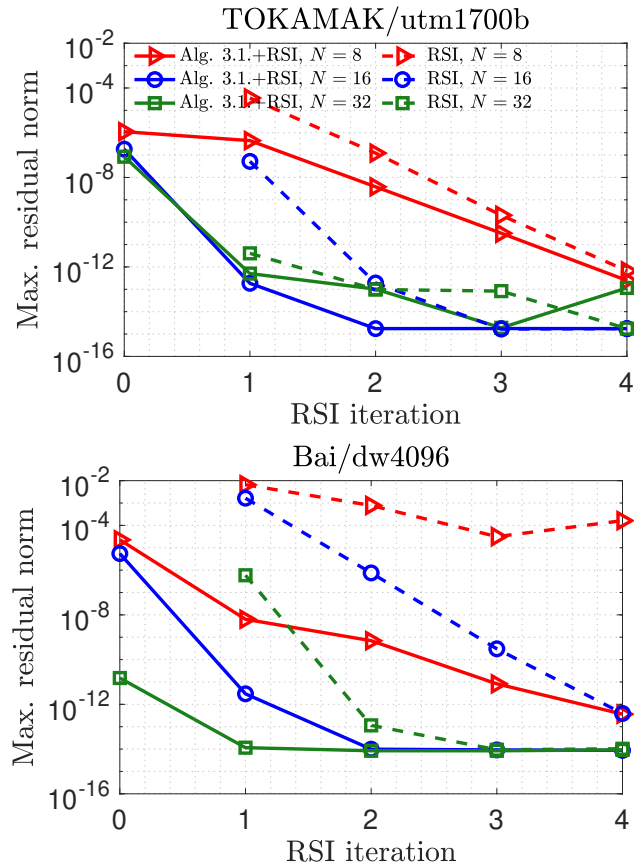


FIG. 5.5. Maximum residual norm achieved at each iteration of RSI as  $N$  varies and  $m = 1.5n_{ev}$ ,  $n_{ev} = 40$ . The values listed at the origin denote the maximum residual norm achieved by Algorithm 3.1 before post-processing by RSI.

550 **6. Conclusion.** This paper presents a class of algorithms for the computation  
 551 of all eigenvalues (and associated eigenvectors) of non-Hermitian matrix pencils lo-  
 552 cated inside a disk. The proposed algorithms approximate the sought eigenpairs by  
 553 harmonic Rayleigh-Ritz projections on subspaces built by computing range spaces  
 554 of rational matrix functions through randomized range finders. These rational ma-  
 555 trix functions are designed so that directions associated with non-sought eigenvalues  
 556 are dampened to (approximately) zero. Moreover, the proposed algorithms do not  
 557 require any a priori estimation of the number of eigenvalues located inside the disk.  
 558 The competitiveness of the proposed algorithms was demonstrated through numerical  
 559 experiments performed on a few test problems.

560 Several research directions are left as future work. One such direction is the ex-  
 561 tension of the algorithms presented in this paper with non-Hermitian Krylov subspace  
 562 iterative solvers and hierarchical preconditioners such as those discussed in [11]. More-  
 563 over, although this paper focused on algorithms, rational filtering eigenvalue solvers  
 564 owe a large portion of their appeal in the ample parallelism they offer, and a dis-  
 565 tributed memory implementation of the proposed technique would be also of interest.  
 566 Another interesting research direction is the extension of the algorithms presented in

567 this paper for the computation of a partial Schur decomposition, or the simultaneous  
568 computation of both left and right eigenvectors.

569 **Acknowledgments.** The authors are grateful to the two anonymous referees for  
570 their helpful comments and suggestions which improved the readability and overall  
571 quality of the present manuscript. The contribution of the first author was partially  
572 supported by the Herman H. Goldstine Postdoctoral Fellowship program of the In-  
573 ternational Business Machines Corporation. The work of Yuanzhe Xi was supported  
574 by NSF grant OAC 2003720. Finally, the authors are indebted to Anthony P. Austin  
575 for his comments on an earlier draft of the present manuscript.

576

## REFERENCES

- 577 [1] H. M. AKTULGA, L. LIN, C. HAINE, E. G. NG, AND C. YANG, *Parallel eigenvalue calcula-*  
578 *tion based on multiple shift-invert Lanczos and contour integral based spectral projection*  
579 *method*, *Parallel Computing*, 40 (2014), pp. 195–212.
- 580 [2] J. ASAKURA, T. SAKURAI, H. TADANO, T. IKEGAMI, AND K. KIMURA, *A numerical method for*  
581 *nonlinear eigenvalue problems using contour integrals*, *JSIAM Letters*, 1 (2009), pp. 52–55.
- 582 [3] A. AUSTIN, P. KRAVANJA, AND L. TREFETHEN, *Numerical algorithms based on analytic function*  
583 *values at roots of unity*, *SIAM Journal on Numerical Analysis*, 52 (2014), pp. 1795–1821.
- 584 [4] A. AUSTIN AND L. TREFETHEN, *Computing eigenvalues of real symmetric matrices with rational*  
585 *filters in real arithmetic*, *SIAM Journal on Scientific Computing*, 37 (2015), pp. A1365–  
586 A1387.
- 587 [5] M. V. BAREL, *Designing rational filter functions for solving eigenvalue problems by contour*  
588 *integration*, *Linear Algebra and its Applications*, 502 (2016), pp. 346 – 365. *Structured*  
589 *Matrices: Theory and Applications*.
- 590 [6] W.-J. BEYN, *An integral method for solving nonlinear eigenvalue problems*, *Linear Algebra and*  
591 *its Applications*, 436 (2012), pp. 3839–3863.
- 592 [7] R. F. BOISVERT, R. POZO, K. REMINGTON, R. F. BARRETT, AND J. J. DONGARRA, *Matrix*  
593 *market: a web resource for test matrix collections*, in *Quality of Numerical Software*,  
594 Springer, 1997, pp. 125–137.
- 595 [8] A. BOSE, V. KALANTZIS, E.-M. KONTOPOULOU, M. ELKADY, P. PASCHOU, AND P. DRINEAS,  
596 *Terapca: a fast and scalable software package to study genetic variation in tera-scale*  
597 *genotypes*, *Bioinformatics*, 35 (2019), pp. 3679–3683.
- 598 [9] T. A. DAVIS AND Y. HU, *The University of Florida sparse matrix collection*, *ACM Trans. Math.*  
599 *Softw.*, 38 (2011), pp. 1:1–1:25.
- 600 [10] E. DI NAPOLI, E. POLIZZI, AND Y. SAAD, *Efficient estimation of eigenvalue counts in an*  
601 *interval*, *Numerical Linear Algebra with Applications*, 23 (2016), pp. 674–692.
- 602 [11] G. DILLON, V. KALANTZIS, Y. XI, AND Y. SAAD, *A hierarchical low rank Schur complement*  
603 *preconditioner for indefinite linear systems*, *SIAM Journal on Scientific Computing*, 40  
604 (2018), pp. A2234–A2252.
- 605 [12] P. DRINEAS AND M. W. MAHONEY, *Randnla: randomized numerical linear algebra*, *Communi-*  
606 *cations of the ACM*, 59 (2016), pp. 80–90.
- 607 [13] L. GIRAUD AND J. LANGOU, *When modified gram-schmidt generates a well-conditioned set of*  
608 *vectors*, *IMA Journal of Numerical Analysis*, 22 (2002), pp. 521–528.
- 609 [14] G. GOLUB AND W. KAHAN, *Calculating the singular values and pseudo-inverse of a matrix*,  
610 *Journal of the Society for Industrial and Applied Mathematics, Series B: Numerical Anal-*  
611 *ysis*, 2 (1965), pp. 205–224.
- 612 [15] S. GÜTTEL, E. POLIZZI, P. T. P. TANG, AND G. VIAUD, *Zolotarev quadrature rules and load*  
613 *balancing for the FEAST eigensolver*, *SIAM Journal on Scientific Computing*, 37 (2015),  
614 pp. A2100–A2122.
- 615 [16] N. HALKO, P.-G. MARTINSSON, AND J. A. TROPP, *Finding structure with randomness: Prob-*  
616 *abilistic algorithms for constructing approximate matrix decompositions*, *SIAM Review*, 53  
617 (2011), pp. 217–288.
- 618 [17] V. HERNANDEZ, J. E. ROMAN, AND A. TOMAS, *Restarted lanczos bidiagonalization for the svd*  
619 *in slepc*.
- 620 [18] S. IWASE, Y. FUTAMURA, A. IMAKURA, T. SAKURAI, AND T. ONO, *Efficient and scalable cal-*  
621 *culatation of complex band structure using Sakurai-Sugiura method*, in *Proceedings of the*  
622 *International Conference for High Performance Computing, Networking, Storage and Anal-*  
623 *ysis*, 2017, pp. 1–12.



- 624 [19] Z. JIA, *The convergence of harmonic Ritz values, harmonic Ritz vectors and refined harmonic*  
625 *Ritz vectors*, Mathematics of Computation, 74 (2005), pp. 1441–1456.
- 626 [20] V. KALANTZIS, *Domain decomposition algorithms for the solution of sparse symmetric gener-*  
627 *alized eigenvalue problems*, PhD Thesis, University of Minnesota, (2018).
- 628 [21] V. KALANTZIS, J. KESTYN, E. POLIZZI, AND Y. SAAD, *Domain decomposition approaches for*  
629 *accelerating contour integration eigenvalue solvers for symmetric eigenvalue problems*, Nu-  
630 *merical Linear Algebra with Applications*, 25 (2018), p. e2154.
- 631 [22] V. KALANTZIS, G. KOLLIAS, S. UBARU, A. N. NIKOLAKOPOULOS, L. HORESH, AND K. L. CLARK-  
632 *SON*, *Projection techniques to update the truncated svd of evolving matrices*, arXiv preprint  
633 *arXiv:2010.06392*, (2020).
- 634 [23] V. KALANTZIS, Y. XI, AND Y. SAAD, *Beyond automated multilevel substructuring: Domain*  
635 *decomposition with rational filtering*, SIAM Journal on Scientific Computing, 40 (2018),  
636 pp. C477–C502.
- 637 [24] J. KESTYN, V. KALANTZIS, E. POLIZZI, AND Y. SAAD, *PFEAST: a high performance sparse*  
638 *eigenvalue solver using distributed-memory linear solvers*, in High Performance Comput-  
639 *ing, Networking, Storage and Analysis, SC16: International Conference for, IEEE*, 2016,  
640 pp. 178–189.
- 641 [25] K. KOLLNIG, P. BIENTINESI, AND E. DI NAPOLI, *Rational spectral filters with optimal conver-*  
642 *gence rate*, arXiv:2001.04184, (2020).
- 643 [26] C. LANCZOS, *An iteration method for the solution of the eigenvalue problem of linear differential*  
644 *and integral operators*, United States Governm. Press Office Los Angeles, CA, 1950.
- 645 [27] R. B. LEHOUCQ, D. C. SORENSEN, AND C. YANG, *ARPACK users' guide: solution of large-scale*  
646 *eigenvalue problems with implicitly restarted Arnoldi methods*, vol. 6, SIAM, 1998.
- 647 [28] R. LI, Y. XI, L. ERLANDSON, AND Y. SAAD, *The eigenvalues slicing library (evsl): Algo-*  
648 *rithms, implementation, and software*, SIAM Journal on Scientific Computing, 41 (2019),  
649 pp. C393–C415.
- 650 [29] R.-C. LI, *Rayleigh quotient based optimization methods for eigenvalue problems*, in Matrix  
651 *Functions and Matrix Equations*, World Scientific, 2015, pp. 76–108.
- 652 [30] E. LIBERTY, F. WOOLFE, P.-G. MARTINSSON, V. ROKHLIN, AND M. TYGERT, *Randomized algo-*  
653 *rithms for the low-rank approximation of matrices*, Proceedings of the National Academy  
654 *of Sciences*, 104 (2007), pp. 20167–20172.
- 655 [31] X. LIU, Y. XI, Y. SAAD, AND M. V. DE HOOP, *Solving the three-dimensional high-frequency*  
656 *helmholtz equation using contour integration and polynomial preconditioning*, SIAM Jour-  
657 *nal on Matrix Analysis and Applications*, 41 (2020), pp. 58–82.
- 658 [32] M. W. MAHONEY AND P. DRINEAS, *Cur matrix decompositions for improved data analysis*,  
659 *Proceedings of the National Academy of Sciences*, 106 (2009), pp. 697–702.
- 660 [33] P.-G. MARTINSSON, *Randomized methods for matrix computations*, The Mathematics of Data,  
661 25, pp. 187–231.
- 662 [34] P.-G. MARTINSSON AND J. TROPP, *Randomized numerical linear algebra: Foundations & algo-*  
663 *rithms*, arXiv preprint arXiv:2002.01387, (2020).
- 664 [35] R. B. MORGAN, *Computing interior eigenvalues of large matrices*, Linear Algebra and its  
665 *Applications*, 154 (1991), pp. 289–309.
- 666 [36] R. B. MORGAN AND M. ZENG, *Harmonic projection methods for large non-symmetric eigen-*  
667 *value problems*, Numerical Linear Algebra with Applications, 5 (1998), pp. 33–55.
- 668 [37] B. N. PARLETT, *The symmetric eigenvalue problem*, vol. 20, SIAM, 1998.
- 669 [38] P. T. PETER TANG AND E. POLIZZI, *FEAST as a subspace iteration eigensolver accelerated by*  
670 *approximate spectral projection*, SIAM Journal on Matrix Analysis and Applications, 35  
671 (2014), pp. 354–390.
- 672 [39] E. POLIZZI, *Density-matrix-based algorithm for solving eigenvalue problems*, Phys. Rev. B, 79  
673 (2009), pp. 115–112.
- 674 [40] V. ROKHLIN, A. SZLAM, AND M. TYGERT, *A randomized algorithm for principal component*  
675 *analysis*, SIAM Journal on Matrix Analysis and Applications, 31 (2010), pp. 1100–1124.
- 676 [41] A. RUHE, *Rational Krylov: A practical algorithm for large sparse nonsymmetric matrix pencils*,  
677 *SIAM Journal on Scientific Computing*, 19 (1998), pp. 1535–1551.
- 678 [42] Y. SAAD, *ILUM: a multi-elimination ILU preconditioner for general sparse matrices*, SIAM  
679 *Journal on Scientific Computing*, 17 (1996), pp. 830–847.
- 680 [43] T. SAKURAI, Y. FUTAMURA, AND H. TADANO, *Efficient parameter estimation and implemen-*  
681 *tation of a contour integral-based eigensolver*, Journal of Algorithms & Computational  
682 *Technology*, 7 (2013), pp. 249–269.
- 683 [44] T. SAKURAI AND H. SUGIURA, *A projection method for generalized eigenvalue problems using*  
684 *numerical integration*, Journal of computational and applied mathematics, 159 (2003),  
685 pp. 119–128.

- 686 [45] T. SAKURAI, H. TADANO, ET AL., *CIRR: a Rayleigh-Ritz type method with contour integral for*  
687 *generalized eigenvalue problems*, Hokkaido Mathematical Journal, 36 (2007), pp. 745–757.
- 688 [46] L. N. TREFETHEN AND J. WEIDEMAN, *The exponentially convergent trapezoidal rule*, SIAM  
689 Review, 56 (2014), pp. 385–458.
- 690 [47] J. WINKELMANN AND E. DI NAPOLI, *Non-linear least-squares optimization of rational filters for*  
691 *the solution of interior hermitian eigenvalue problems*, Frontiers in Applied Mathematics  
692 and Statistics, 5 (2019), p. 5.
- 693 [48] Y. XI AND Y. SAAD, *Computing partial spectra with least-squares rational filters*, SIAM Journal  
694 on Scientific Computing, 38 (2016), pp. A3020–A3045.
- 695 [49] ———, *A rational function preconditioner for indefinite sparse linear systems*, SIAM Journal  
696 on Scientific Computing, 39 (2017), pp. A1145–A1167.
- 697 [50] I. YAMAZAKI, H. TADANO, T. SAKURAI, AND T. IKEGAMI, *Performance comparison of parallel*  
698 *eigensolvers based on a contour integral method and a Lanczos method*, Parallel Comput-  
699 ing, 39 (2013), pp. 280 – 290.
- 700 [51] X. YE, J. XIA, R. H. CHAN, S. CAULEY, AND V. BALAKRISHNAN, *A fast contour-integral eigen-*  
701 *solver for non-Hermitian matrices*, SIAM Journal on Matrix Analysis and Applications,  
702 38 (2017), pp. 1268–1297.
- 703 [52] G. YIN, *A contour-integral based method with Schur–Rayleigh–Ritz procedure for generalized*  
704 *eigenvalue problems*, Journal of Scientific Computing, 81 (2019), pp. 252–270.
- 705 [53] ———, *A harmonic feast algorithm for non-hermitian generalized eigenvalue problems*, Linear  
706 Algebra and its Applications, 578 (2019), pp. 75–94.
- 707 [54] G. YIN, R. H. CHAN, AND M.-C. YEUNG, *A FEAST algorithm with oblique projection for*  
708 *generalized eigenvalue problems*, Numerical Linear Algebra with Applications, 24 (2017),  
709 p. e2092.
- 710 [55] H. ZHA AND H. D. SIMON, *On updating problems in latent semantic indexing*, SIAM Journal  
711 on Scientific Computing, 21 (1999), pp. 782–791.